



Comparison of two metabolomics-platforms to discover biomarkers in critically ill patients from serum analysis



Tiago A.H. Fonseca ^{a,b,c,*}, Cristiana P. Von Rekowski ^{a,b,c}, Rúben Araújo ^{a,b,c}, M. Conceição Oliveira ^d, Gonçalo C. Justino ^d, Luís Bento ^{e,f}, Cecília R.C. Calado ^{b,g}

^a NMS - NOVA Medical School, FCM - Faculdade de Ciências Médicas, Universidade NOVA de Lisboa, Campo Dos Mártires da Pátria 130, 1169-056, Lisbon, Portugal

^b ISEL - Instituto Superior de Engenharia de Lisboa, Instituto Politécnico de Lisboa, Rua Conselheiro Emídio Navarro 1, 1959-007, Lisbon, Portugal

^c CHRC - Comprehensive Health Research Centre, Universidade NOVA de Lisboa, 1150-082, Lisbon, Portugal

^d Centro de Química Estrutural - Institute of Molecular Sciences, Instituto Superior Técnico, Universidade de Lisboa, Av. Rovisco Pais 1, 1049-001, Lisbon, Portugal

^e Intensive Care Department, ULSSJ - Unidade Local de Saúde de São José, Rua José António Serrano, 1150-199, Lisbon, Portugal

^f Integrated Pathophysiological Mechanisms, CHRC - Comprehensive Health Research Centre, NMS - NOVA Medical School, FCM - Faculdade de Ciências Médicas, Universidade NOVA de Lisboa, Campo Mártires da Pátria, 1169-056, Lisbon, Portugal

^g IBB-Institute for Bioengineering and Biosciences, The Associate Laboratory Institute for Health and Bioeconomy (i4HB), Instituto Superior Técnico, Universidade de Lisboa, Av. Rovisco Pais, 1049-001, Lisbon, Portugal

ARTICLE INFO

Keywords:

Metabolomics
Fourier transform infrared spectroscopy
Mass spectrometry
Liquid chromatography

ABSTRACT

Serum metabolome analysis is essential for identifying disease biomarkers and predicting patient outcomes in precision medicine. Thus, this study aims to compare Ultra-High Performance Liquid Chromatography-High-Resolution Mass Spectrometry (UHPLC-HRMS) with Fourier Transform Infrared (FTIR) spectroscopy in acquiring the serum metabolome of critically ill patients, associated with invasive mechanical ventilation (IMV), and predicting death. Three groups of 8 patients were considered. Group A did not require IMV and survived hospitalization, while Groups B and C required IMV. Group C patients died a median of 5 days after sample harvest. Good prediction models were achieved when comparing groups A to B and B to C using both platforms' data, with UHPLC-HRMS showing 8–17 % higher accuracies ($\geq 83\%$). However, developing predictive models using metabolite sets was not feasible when comparing unbalanced populations, i.e., Groups A and B combined to Group C. Alternatively, FTIR-spectroscopy enabled the development of a model with 83 % accuracy. Overall, UHPLC-HRMS data yields more robust prediction models when comparing homogenous populations, potentially enhancing understanding of metabolic mechanisms and improving patient therapy adjustments. FTIR-spectroscopy is more suitable for unbalanced populations. Its simplicity, speed, cost-effectiveness, and high-throughput operation make it ideal for large-scale studies and clinical translation in complex populations.

1. Introduction

Metabolomics encompasses the systematic study of small molecules that belong to specific biological systems, with molecular weights usually under 1500 Da. These small molecules are part of metabolic pathways associated to normal and pathological processes [1], as primary, intermediate and/or end products of the metabolism [2]. Therefore, metabolomics is a representation of an individual's phenotype [3], reflecting all interactions and biological processes that occur

downstream of genomics, transcriptomics, and proteomics [4,5]. Consequently, metabolomics has been intensively explored in the context of precision medicine [6], to discover biomarkers associated with defined physiological states [7–10], such as in ageing processes [11], impact of microbiome [12], disease diagnosis and prognosis, including cancer [13,14], autoimmune diseases [15–17], infection [2], genetic disorders [18], psychiatric diseases [19] and response to drugs [20,21].

Metabolomics of biofluids has the advantage of using samples that

* Corresponding author. NMS - NOVA Medical School, FCM - Faculdade de Ciências Médicas, Universidade NOVA de Lisboa, Campo dos Mártires da Pátria 130, 1169-056, Lisbon, Portugal.

E-mail addresses: tiago.alexandre.hf@gmail.com (T.A.H. Fonseca), crisvr66@hotmail.com (C.P. Von Rekowski), rubenalexandredinisoraujo@gmail.com (R. Araújo), conceicao.oliveira@tecnico.ulisboa.pt (M.C. Oliveira), goncalo.justino@tecnico.ulisboa.pt (G.C. Justino), luis.bento@ulssjose.min-saude.pt (L. Bento), cecilia.calado@isel.pt (C.R.C. Calado).

are obtained through non-invasive or minimal invasive approaches, in opposition to tissue-based analyses (e.g., biopsies), while still reflecting the physiological state of the system. From all the biofluids, peripheral blood presents various advantages, since it is a closer representation of the system general state, in comparison to other biofluids, e.g., saliva and urine, that can be more representative of specific diseases from the oral cavity or the urinary system, respectively, and, in contrast with other biofluids, such as the cerebrospinal, it presents less associated risks. For all that, there are numerous studies focusing serum or plasma metabolomics [22–25].

The most employed methods for analysing the metabolome of a system involve a two-step process. First, metabolites present in the samples are separated using techniques such as Ultra-High Performance Liquid Chromatography (UHPLC). Subsequently, separated molecules are analysed using high-resolution mass spectrometry (HRMS), either in a full scan (MS) or in a tandem (MS/MS) approach. While UHPLC effectively isolates a wide range of analytes, HRMS exhibits exceptional sensitivity in detecting and quantifying them. This analytical approach allows for the identification of a broad diversity of metabolites, covering, for instance, three to five orders of magnitude, detecting concentrations lower than 0.01 % of the highest metabolite concentration [26]. Identifying the metabolites associated with the system can also facilitate the discovery of the underlying metabolic pathways and how they respond to external stimuli, such as therapeutic interventions [27]. This process strongly contributes to the development of sensitive and specific biomarkers for diagnosis and prognosis, as well as revealing new sub-types of diseases and potential new therapeutic approaches [28].

Despite the considerable potential of these platforms, they necessitate costly and advanced equipment, entail a time-intensive process, include intricate data processing steps, and the technical complexity introduces numerous variables affecting the identified metabolites [2, 29]. For all of that, many of these omics studies involve a small number of patients, which may not adequately represent the diversity of patients in clinical settings [30], limiting their translation to real-world clinical scenarios. Hence, there exists a pressing need for alternative techniques that, albeit with lower resolution, can be employed in a more simple, economic, and high-throughput manner. These attributes can greatly enhance the technique application to large-scale studies. An example of such technique is Fourier Transform Infrared (FTIR) spectroscopy.

FTIR spectroscopy operates by detecting the vibrations of molecular bonds, thereby providing valuable insights into the samples molecular composition [31–33]. The mid-infrared region (MIR) offers several advantages over the near-infrared region (NIR) of the spectra, since MIR focuses on fundamental vibrations, while NIR primarily detects overtones and combinations of fundamental vibrations. These overtones are typically less intense and result in broader bands compared to the sharper peaks observed in MIR spectra. Moreover, when dealing with complex biological samples, NIR predominantly identifies bonds involving hydrogen, whereas MIR can detect a broader range of bonds [34]. An additional advantage of FT-MIR spectroscopy is its adaptability to various operation setups, including integration with automatic microplates readers, allowing for economical and high-throughput analyses. For instance, even with sample volumes as small as 5 μ L and just after a single dehydration step, one can automatically analyse samples in 384 well-microplates spanning from 400 to 4000 cm^{-1} [35,36]. For all of that, FT-MIR spectroscopy has gathered substantial attention as an analytical tool, particularly for human biofluid analysis [37,38]. This technique, associated to machine learning algorithms, has been explored to develop predictive models with high sensitivity and specificity, applied to, e.g., cancer [32], infectious diseases [33], and neurodegenerative diseases [39], among others [40–42].

Due to the significant promise and complementary nature of UHPLC-HRMS and FT-MIR spectroscopy, several independent studies have delved into their applications for human biofluids analysis. However, most publications have primarily concentrated on utilizing FT-MIR

spectroscopy as a rapid assessment tool for sample preparation, with the subsequent metabolomics analysis carried out using UHPLC-HRMS or equivalent methods [43,44].

The primary objective of the present study was to conduct a comparative analysis between these two analytical platforms, UHPLC-HRMS and FT-MIR spectroscopy, for the assessment of the serum metabolome of critically ill patients admitted to an intensive care unit (ICU). This demographic was selected due to the inherent challenges associated with biomarker discovery in exceedingly heterogeneous and dynamic populations. Patients admitted to ICU present a considerable diversity regarding admission motives, demographics, comorbidities, disease severity, while presenting rapid and dynamic changes in their physiological status [45–48]. A total of 24 patients with Coronavirus Disease 2019 (COVID-19), were assembled in three groups of eight patients each (A, B and C). Group A patients did not require invasive mechanical ventilation (IMV) and were later discharged from the ICU; patients in Group B required IMV and were also discharged from ICU; Group C patients were under IMV and died a median of five days after the current analysis. Predictive models, using data from the two analytical platforms, were developed, considering the following three comparisons: A vs. B, to predict the more severe disease state of Group B (that required IMV); B vs C, and A plus B vs. C, to predict death in the ICU, considering only patients under IMV (B vs. C), or a control group of patients comprising both those necessitating and those not requiring IMV (A plus B vs. C).

2. Materials and methods

2.1. Study design

Peripheral whole blood samples from 24 male COVID-19 patients hospitalized at the ICU from *Unidade Local de Saúde de São José* (Lisbon, Portugal) were collected and analysed according to legal and ethical requirements (project number approved by the Hospital Ethics Commission: 1043/2021, 20/05/2020). All patients in the study were diagnosed with COVID-19 through real-time polymerase chain reaction (RT-PCR) testing.

Demographic and clinical profiles of the cohort were obtained through the hospital's medical record system. The cohort was stratified into three distinct groups, denoted as Groups A to C, each comprising eight patients, according to the following:

Group A: patients who did not require IMV and were discharged from the ICU.

Group B: patients who underwent IMV and were discharged from the ICU.

Group C: patients who underwent IMV and that died in the ICU, in average seven days after sample harvest.

When IMV was required, patients underwent rapid sequence intubation. The IMV modality used was pressure regulated volume control with a lung protection strategy (tidal volume less than 6 mL/kg and plateau pressure less than 30 cm H₂O). Patients were sedated and given neuromuscular blockers during the first 48 h. After this period, the neuromuscular blockers were stopped, and sedation was adjusted to achieve a Richmond Agitation-Sedation Scale (RASS) score of 0 to -2.

2.2. Sample preparation for Serum metabolome analysis

Serum was obtained from blood by centrifugation at 3000 rpm for 10 min and was subsequently kept at -80 °C until analysis. The metabolome was acquired from serum samples following the methodology outlined by Fonseca et al. [44]. Briefly: samples and solvents were maintained on ice throughout the procedure. A volume of 75 μ L of serum was mixed with 265 μ L of a solvent mixture composed of methanol, acetonitrile, and water in a ratio of 2:2:1 (v/v). All solvents utilized were

of LC/MS grade quality (Fisher Chemical). The resulting mixture was vortexed and subsequently centrifuged at 18,000×g for 15 min at 4 °C (Mixtasel centrifuge, J.P. Selecta). Supernatants were carefully collected and stored at –80 °C until analysis.

2.3. UHPLC-HRMS

Analyses were performed using an Elute UHPLC system composed of an Elute UHPLC HPG 1300 pump with two pairs of serial-coupled, individually controlled, linear drive pump heads, an Elute autosampler, and an Elute column CSV preheater oven, coupled to an Impact II QqTOF mass spectrometer with an electrospray ion source (Bruker Daltonics GmbH & Co.) (UHPLC-ESI-HRMS). Each sample was processed by two chromatographic modes, Reverse-Phase (RP) and Hydrophilic Interaction Chromatography (HILIC), in both positive and negative ionization modes. In each of these four analytical configurations, 3 full scan analyses were collected for each sample, together with one MS/MS scan.

UHPLC RP system was based on a Luna 2.5 μm C18(2)-HST column (100 Å, 150 × 2 mm, Phenomenex) at a constant temperature of 40 °C, and a gradient elution was used at a flow rate of 250 μL/min as follows (mobile phase A, 0.1 % formic acid in water; mobile phase B, 0.1 % formic acid in acetonitrile): 0.0–0.5 min 0 % B, 0.5–1.5 min 0–20 % B, 1.5–4.0 min 20–60 % B, 4.0–6.0 min 60–100 % B, 6.0–9.0 min 100 % B, 9.0–10.0 min 100–0 % B, and 10.0–15.0 min 0 % B.

For HILIC separations, an XBridge BEH Amide XP column (130 Å, 2.5 μm, 150 × 2.1 mm, Waters) was used at a constant temperature of 40 °C. With a flow rate of 250 μL/min, a gradient elution of 10 mM ammonium acetate in water containing 0.1 % acetic acid (A) and 10 mM ammonium acetate in acetonitrile containing 2 % water and 0.1 % acetic acid (B) was applied as follows: 0–2 min 90 % B, 2–6 min 90–70 % B, 6–9 min 70–30 % B, 9–13 min 30 % B, 13–18 min 30–90 % B, 18–22 min 90 % B.

MS acquisition parameters were set as follows: capillary voltage of 3 kV (ESI-) or 4.5 kV (ESI+), end plate offset of 500 V, nebulizer of 4.0 bar, dry gas flow of 8.0 L/min, and dry heater temperature of 200 °C. Spectral acquisition was performed with an absolute threshold of 25 counts per 1000. For auto MS/MS data acquisition, the capillary voltage was set at 4.5 (ESI+) or 3.5 kV (ESI-) with an end plate offset of 500 V, a nebulizer pressure of 4.0 bar, a dry gas flow of 8.0 L/min, and a heater temperature of 200 °C. Spectra acquisition was performed with a threshold of 20 counts per 1000, a cycle time of 3.0 s with exclusion after 3 spectra, and release after 1.00 min. Calibration of the mass spectrometer was performed through direct infusion with a 10 mM sodium formate/acetate solution introduced to the ion source via a 20 μL loop using the high-precision calibration mode. For internal calibration in each sample, an initial 10 s calibration segment was acquired.

All acquisitions were performed with a *m/z* range from 50 to 1300 with a 3 Hz spectra rate. Three full scans and one auto MS/MS scan were performed for each sample using both positive and negative ionization mode. A 25 μM solution containing quercetin, L-tryptophan (indole-d₅), L-valine (d₈), sulfolene (d₄), and *N,N*-dimethyl-d₆-glycine HCl was prepared and used as quality control. This quality control sample was analysed every 6 h to ensure that chromatographic resolution and spectrometer detection did not change throughout time.

Acquired MS data were internally calibrated relative to the infused calibrant using Data Analysis (version 4.5, Bruker Daltoniks), converted to mzXML using ProteoWizard MSConvert [49], and uploaded to the XCMS server [50–53], where data processing (including feature detection, retention time correction, peak alignment, and METLIN annotation), pairwise sample comparison, multimodal analysis (independent of separation and acquisition modes), and global metanalysis were performed. The XCMS parameters employed in the study were adapted from Fonseca et al. [44], and significant differences in metabolites between patient groups were identified using thresholds of *p* < 0.01, *p* < 0.05, or *p* < 0.001.

The diseases enrichment analysis was performed against 344 metabolite sets describing human disease signatures in blood using MetaboAnalyst [54–56].

2.4. FTIR Spectroscopy

A total 5 μL of each sample was plated in a 384-well silicon microplate (Bruker Optics GmbH & Co. KG) and then placed on a desiccator under vacuum for 2.5 h. Spectra were acquired with an FTIR spectrometer (Vertex 70, Bruker Optics GmbH & Co. KG) associated to an HTS-XT system (Bruker Optics GmbH & Co. KG). Each spectrum resulted from 64 scans with a 2 cm^{−1} resolution between 800 and 4000 cm^{−1}. The first microplate's well was kept empty as its spectrum was used as background, according to the HTS-XT manufacturer instructions. Each sample was analysed in triplicate.

FTIR-spectra were pre-processed by atmospheric correction and baseline corrections with OPUS software (version 6.5, Bruker Optics GmbH & Co. KG). Spectra normalization was conducted using The Unscrambler X (CAMO software AS, version 10.4, Oslo, Norway).

2.5. Multivariate analysis

Principal component analysis (PCA), Linear Discriminant Analysis (LDA), or an PCA-LDA of UHPLC-HRMS and FTIR spectral data were conducted using The Unscrambler X. Specifically, for FTIR-spectral data, which contains more variables than samples, a preliminary PCA was conducted before LDA. In contrast, unless otherwise specified, UHPLC-HRMS results were analysed by LDA.

Classification models (LDA or PCA-LDA) were developed to distinguish patients' groups, based on seven different sets of metabolites in the case of UHPLC-HRMS data, and based on different spectra pre-processing in the case of FTIR data, for each of the three comparisons between groups. The samples were divided between train and test sets, with a distribution of 75 % in the train set and 25 % in the test set. This process was repeated 4 times, where in each process no samples were used more than once in the test set. This resulted in a total of 84 models from UHPLC-HRMS analysis and 96 models from FTIR analysis. For each comparison, and set of metabolites, the average performance of the 4 train/test models was presented.

2.6. Other Statistical analysis

Regarding patients' demographics and clinical characteristics, continuous variables were expressed by their medians and interquartile range (25th percentile–75th percentile), and categorical data were presented as absolute frequencies and respective percentages. Regarding nominal variables, comparisons between independent groups were conducted using non-parametric chi-square or Fisher's exact tests (if the conditions for the chi-square test were not met). Continuous variables were compared using the Mann–Whitney *U* test. For other continuous variables, namely FTIR-spectral bands, data were presented as mean and standard deviation (S.D.). These analyses were conducted on IBM SPSS Statistics software, version 26 (IBM Corp., New York, United States).

Comparisons between groups, using data from FTIR-spectroscopy (with spectra previously pre-processed with atmospheric and baseline correction and with unit vector normalization) and UHPLC-HRMS, were performed using the independent samples Mann–Whitney *U* test and Welch's *t*-test, respectively. To reduce false positives (Type I errors) in the FTIR-spectral bands comparisons, the Holm–Bonferroni correction was applied, which better controls the family-wise error rate while maintaining statistical power across multiple tests. Statistical significance was set for a two-sided *p*-value of less than 0.05.

3. Results

Each of the three patient groups (A, B, and C), comprised eight

patients, all critically ill and admitted to the ICU (Table 1), where patients from Group A did not require IMV, and patients in Groups B and C were under IMV at the time of the current analysis. Patients of Group C died a median of five days after sample collection. Consequently, the illness severity escalates progressively from patients in Group A to those in Group C. Analysis of the serum metabolome, as acquired by UHPLC-HRMS and FTIR spectroscopy, were compared between:

Group A with Group B, reflecting the impact of IMV.
Group B with Group C, to predict death of group C, and considering that all patients were under IMV.

Groups A and B together, in comparison to Group C, to predict death of Group C, and considering a more heterogenous control group, i.e., including patients with and without IMV.

To minimize the impact of confounding variables, patients for each group were selected to ensure no significant differences in demographic variables (e.g., age and gender) and comorbidities between the groups at a 5 % significance level (Table 1). Additionally, no significant impact of medications administered 48 h before sample analysis was observed between groups, except for fentanyl ($p < 0.001$), propofol ($p < 0.001$), and norepinephrine ($p = 0.003$) between groups A and B. These medications are associated with the IMV procedure applicable to group B patients. The remaining therapeutic regimen, outlined in Table S1, showed no statistical differences between groups and includes commonly used ICU medications for managing trauma, sepsis, cardiovascular issues, respiratory distress, and infections. These medications range from antivirals like acyclovir, antibiotics such as amoxicillin-clavulanic acid and azithromycin, to anticoagulants like enoxaparin and heparin, sedatives like midazolam, and pain management drugs such as morphine. They are standard in critical care for stabilizing patients and addressing complications from severe illness or injury.

3.1. UHPLC-HRMS: univariate data analysis and principal component analysis

The molecular features, i.e., the m/z peaks, obtained from both RP and HILIC columns using the UHPLC-HRMS platform, were determined (Table 2). The total number of features were similar between all

Table 2

Molecular Features (m/z peaks) detected by UHPLC-HRMS in each group of patients.

HPLC column	Group A Discharged	Group B IVM & Discharged	Group C IVM & Deceased
RP ESI+	7420	7467	7563
RP ESI-	3903	3995	4051
HILIC ESI+	7478	7507	7526
HILIC ESI-	3847	3902	3936
Total number	22648	22871	23076

patients' groups, where positive ionization mode (ESI+) presented approximately twice the number of features relative to the negative ionization mode (ESI-), in agreement with other authors [44,57,58]. Pairwise comparisons of these features pointed significantly different metabolites between groups (Fig. 1 to 4, Supplementary Tables S1–S3), as discussed in the following sections.

3.1.1. Group a versus group B

When comparing Group A with B (without IMV vs. with IMV), 64 significantly different features were detected, which corresponded to 28 putative metabolites ($p < 0.001$) (Fig. 1A, Table S2), where patients undergoing IMV (Group B) exhibited:

Up-regulated metabolites: carbohydrates and carbohydrate conjugates, N4-(β -N-acetyl-D-glucosaminyl)-L-asparagine, α -D-glucose, 3-keto-L-gulonate, N-acetyl- β -neuraminate, xylitol and myo-inositol; the hydroxy acids (R)-lactate and L-gulonate; the lipidic molecules octanoate and calcitriol (vitamin D); thiamine (vitamin B1), L-ascorbate (vitamin C), 5-methoxytryptophol and S-adenosyl-L-homocysteine.

Down-regulated metabolites: the lipids (4Z,7Z,10Z,13Z,16Z,19Z)-docosahexaenoate and arachidonate; the carboxylic acids 4-methyl-2-oxopentanoate and fumarate; the pyrimidine and pyridine derivatives 5,6-dihydrothymine and 3-pyridylacetate, respectively; the organic carbonic acids 3-ureidopropionate and 3-ureido-isobutyrate, imidazole and imidazopyrimidines (urocanate and urate, respectively), and 4-acetamidobutanal and (S)-3-methyl-2-oxopentanoate.

The PCA based on these 28 metabolites presented a good separation on PC1 vs. PC2 score-plot between patient groups, highlighting that

Table 1

Patient's demographic and clinical data, by Group, and comparisons between them.

	Group A	Group B	Groups A + B	Group C	Group A vs B	Group B vs C	Group A + B vs C p values
	Discharged (n = 8)	IVM & Discharged (n = 8)	Discharged (n = 16)	IVM & Deceased (n = 8)	p values	p values	
Age; years	52.0 (43.3–62.0)	55.0 (51.0–66.8)	53.5 (50.3–62.3)	65.0 (60.5–67.8)	0.328	0.234	0.061
Comorbidities	6 (75 %)	7 (88 %)	13 (81 %)	5 (63 %)	–	0.569	0.362
Arterial hypertension	2 (25 %)	6 (75 %)	8 (50 %)	3 (38 %)	0.132	0.315	0.679
Obesity	2 (25 %)	4 (50 %)	6 (38 %)	2 (25 %)	0.608	0.608	0.667
Diabetes	2 (25 %)	3 (38 %)	5 (31 %)	3 (38 %)	–	–	–
Dyslipidemia	2 (25 %)	2 (25 %)	4 (25 %)	2 (25 %)	–	–	–
Chronic respiratory illness	2 (25 %)	2 (25 %)	4 (25 %)	3 (38 %)	–	–	0.647
IMV	0 (100 %)	8 (100 %)	8 (50 %)	8 (100 %)	<0.001	–	0.022
High Flow Oxygen therapy	8 (100 %)	2 (25 %)	10 (63 %)	2 (25 %)	0.007	–	0.193
Total time at the ICU; days	7.0 (5.0–8.8)	13.5 (10.5–22.0)	10.0 (6.5–14.5)	12.5 (8.0–15.3)	0.002	0.328	0.490
Time between ICU admission and sample harvest; days	5.0 (1.5–6.0)	5.5 (3.0–9.8)	5.0 (3.0–7.0)	4.5 (3.3–7.8)	0.382	0.798	0.834
Time between sample harvest and death; days	–	–	–	5.0 (4.3–11.5)	–	–	–
Total time with IMV; days	–	8.0 (5.0–13.5)	5.0 (0.0–11.0)	9.5 (7.3–15.0)	–	0.645	0.574
Time with IMV when sample was harvested; days	–	4.0 (2.3–9.8)	4.0 (2.3–9.8)	3.5 (3–6.8)	–	0.574	0.076
Fentanyl	0 (0 %)	7 (88 %)	7 (44 %)	7 (88 %)	<0.001	–	0.079
Norepinephrine	0 (0 %)	6 (75 %)	6 (38 %)	5 (63 %)	0.003	–	0.390
Propofol	0 (0 %)	7 (88 %)	7 (44 %)	7 (88 %)	<0.001	–	0.079
Erythromycin	0 (0 %)	5 (63 %)	5 (31 %)	4 (50 %)	0.013	–	0.412

Continuous variables are presented as median (P25–P75), and categorical variables are presented as n (%).

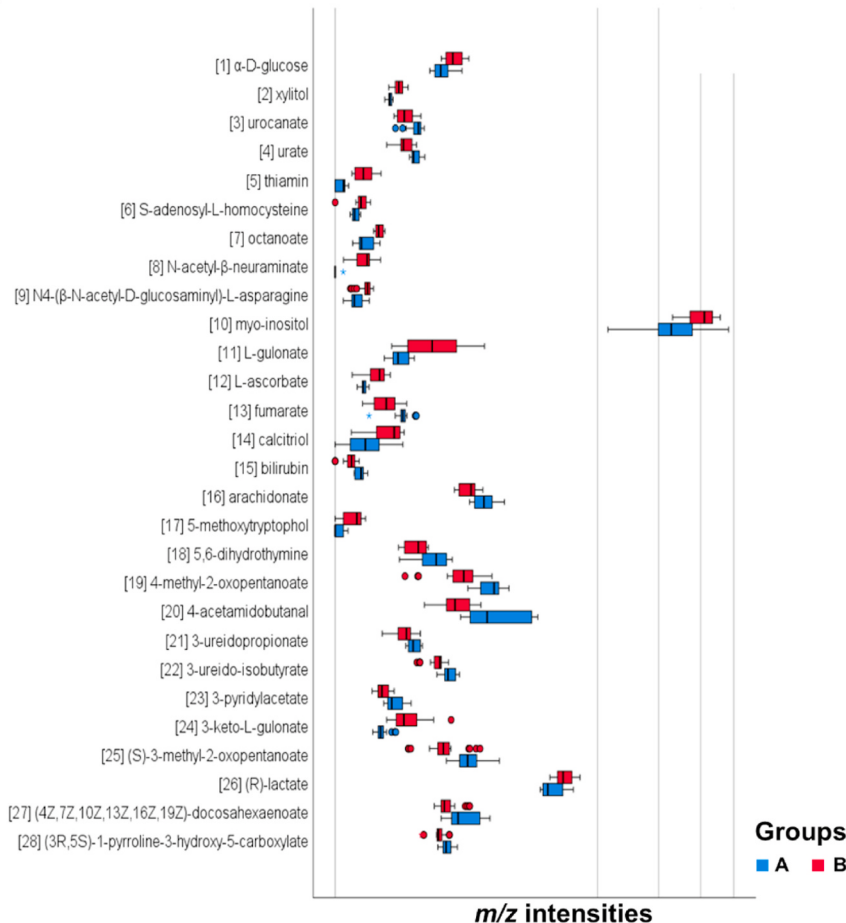
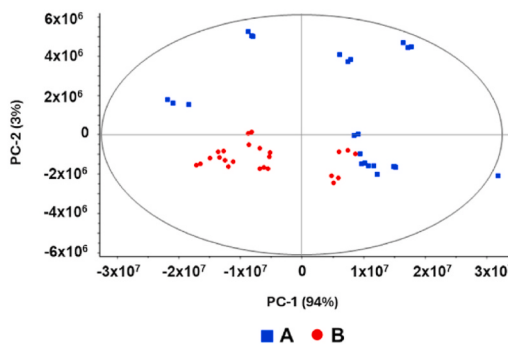
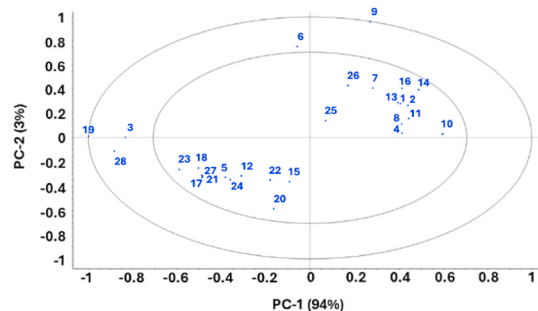
A**B****C**

Fig. 1. Impact of IMV on the patients' serum metabolome. **A:** Intensities of the 28 statistically different metabolites between Group A and B ($p < 0.001$), detected by UHPLC-HRMS. The x axis was scaled to the power of 0.3 for better visualization of the boxplots. **B:** PCA from the 28 metabolites. **C:** Correlation loadings from both PC1 and PC2, with numbers corresponding to the metabolites listed in panel A. Exterior and interior ellipse corresponds to 100 % and 50 % explained variance, respectively.

these metabolites represent the impact of IMV (Fig. 1B). The loading vector of PC1 and PC2, representing 97 % of explained variance (Fig. 1C), indicated that the most representative metabolites for the patients separation according to their group were the pyridylacetate and acetomidobutanal (localized on the positive side of the PC2 axis, thus associated with decreased values for Group B); and myo-inositol, lactate and glucose (located on the negative side of the PC1 axis, suggesting increased values for Group B).

3.1.1.1. Group B versus Group C.

When comparing Group B (under IMV) with C (under IMV, deceased), 64 differentially expressed features were

detected, associated to 39 putative metabolites (7 of them at $p < 0.001$ and 32 at a p-value between 0.001 and 0.05) (Fig. 2. A, Table S3). Deceased patients (Group C) presented:

- Higher values of some lipids (octanoate, docosahexaenoate, arachidonate, 6-methoxy-3-methyl-2-all-trans-decaprenyl-1,4-benzoquinol, and icosapentaenoate), purine nucleosides and nucleotide (inosine, 3'-dephospho-CoA and flavine mononucleotide (FMN)), hydroxy acids (lactate, gulonate and malate), keto acids (4-fumaryl-acetoacetate and pyruvate), organooxygen compounds (ribose-1-arsenate, N-acetyl-β-neuraminate and N-formylkynurenine),

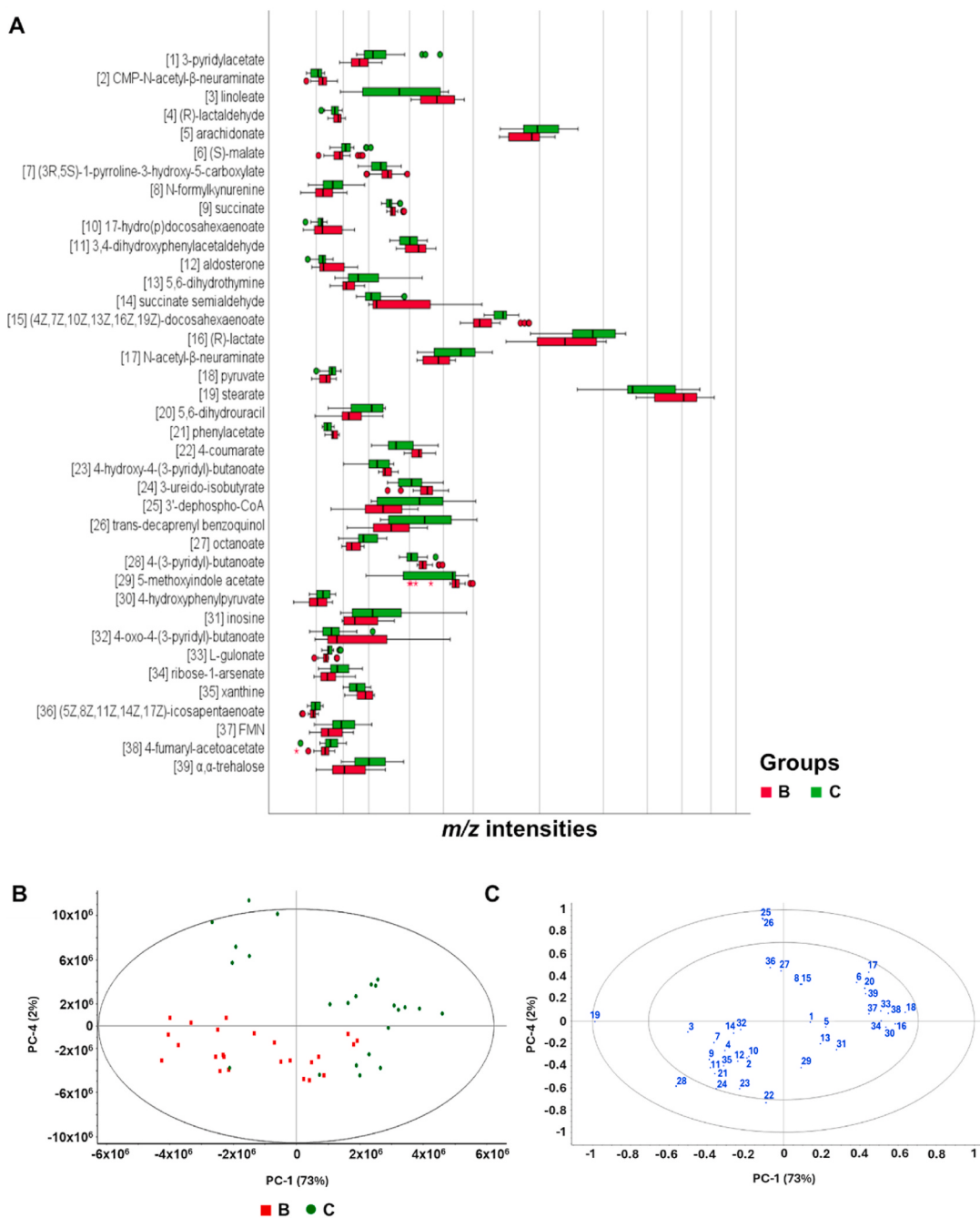


Fig. 2. Impact of mortality on the patients' serum metabolome, based on patients under IMV. **A:** Intensities of the 39 statistically different metabolites between Group B and C ($p < 0.05$), detected by UHPLC-HRMS. The x axis was scaled to the power of 0.3 for better visualization of the boxplots. **B:** PCA from the 39 metabolites. **C:** Correlation loadings from both PC1 and PC4, with numbers corresponding to the metabolites listed in panel A. Exterior and interior ellipse corresponds to 100 % and 50 % explained variance, respectively. Abbreviations: trans-decaprenyl benzoquinol – 6-methoxy-3-methyl-2-all-trans-decaprenyl-1,4-benzoquinol.

diazines (dihydrouracil and dihydrothymine), the carbohydrate trehalose, the benzenoid 4-hydroxyphenylpyruvate and the pyridine pyridylacetate.

- Lower values of other lipids (stearate, succinate semialdehyde, 17-hydro(p)docosahexaenoate, linoleate and aldosterone), benzenoids (phenylacetate and 3,4-dihydroxyphenylacetalddehyde), carboxylic acids (succinate, (3R,5S)-1-pyrroline-3-hydroxy-5-carboxylate), the purine degradation byproduct xanthine and the nucleotide CMP-N-acetyl- β -neuraminate, pyridines (4-(3-pyridyl)-butanoate, 4-hydroxy-4-(3-pyridyl)-butanoate) keto acid (4-oxo-4-(3-pyridyl)-butanoate), the organooxygen lactaldehyde and 3-ureido-isobutyrate, 5-methoxyindole acetate and 4-coumarate.

The PCA based on those 39 metabolites presented a good separation on PC1 vs. PC4 score plot (Fig. 2B). According to the PCA loadings (Fig. 2C), the following 5 metabolites contributed the most to the separation between groups: methoxy-methyl-all-trans-decaprenylbenzoquinol ($p < 0.001$) and dephospho-coenzyme A ($p = 0.0011$), with positive PC4 values, i.e., with higher values for deceased patients; and stearate ($p = 0.00031$), 4-(3-pyridyl)-butanoate ($p < 0.001$), and coumarate ($p = 0.0045$), with negative PC1 values, i.e., with lower values for deceased patients deceased patients, at a global $p < 0.005$.

3.1.1.2. Group A plus B versus Group C. The comparison between Group A and B (without and with IMV) to Group C (with IMV and deceased),

resulted in 64 m/z peaks corresponding to 39 putative metabolites (35 at $p < 0.001$ and 4 at $0.001 < p < 0.01$) (Fig. 3A, Table S4), where deceased patients (Group C) presented:

- Higher values of carbohydrates (β -D-glucose, N-acetyl- β -neuraminate, L-xylulose, α,α -trehalose, ribose-1-arsenate and xylitol), some lipids (oleate, arachidonate, stearate, octanoate, ADP ribose 1",2"-cyclic phosphate and 6-methoxy-3-methyl-2-all-trans-decaprenyl-1,4-benzoquinol), amino acids (3,3'-diiodothyronine and L-arginine), nucleotide/nucleoside derivates (5-amino-1-(5-phospho-D-ribosyl)imidazole-4-carboxamide, FMN, 2'-deoxyuridine and cytidine), keto acids (acetoacetate and pyruvate) and aldehyde analogue of pyruvate methylglyoxal and hydroxy acids (lactate and malate).
- Lower values of carbohydrate derivate β -L-fucose 1-phosphate, some lipids (linoleate, α -tocopherol, sphingosine 1-phosphate, (25R)-5 β -

cholestane-3 α ,7 α ,12 α ,26-tetraol), the hydroxy fatty acid (R)-mevalonate diphosphate, the amino acid lysine, nucleotides/nucleosides (GDP- α -D-glucose and CMP-N-acetyl- β -neuraminic acid), purine (xanthine), keto acid (4-methyl-2-oxopentanoate), as well as metanephrine, L-ornithine, 3-ureido-isobutyrate porphobilinogen and 5-methoxyindoleacetaldehyde.

The PCA performed with these metabolites did not reveal a clear separation between discharged and deceased patients (Fig. 3B). However, patients from Group A were all in the quadrants with positive PC1 values, indicating that the PCA separated patients based on IMV status.

3.2. UHPLC-HRMS: LDA or PCA-LDA predictive models

Supervised LDA or PCA-LDA models were developed based on

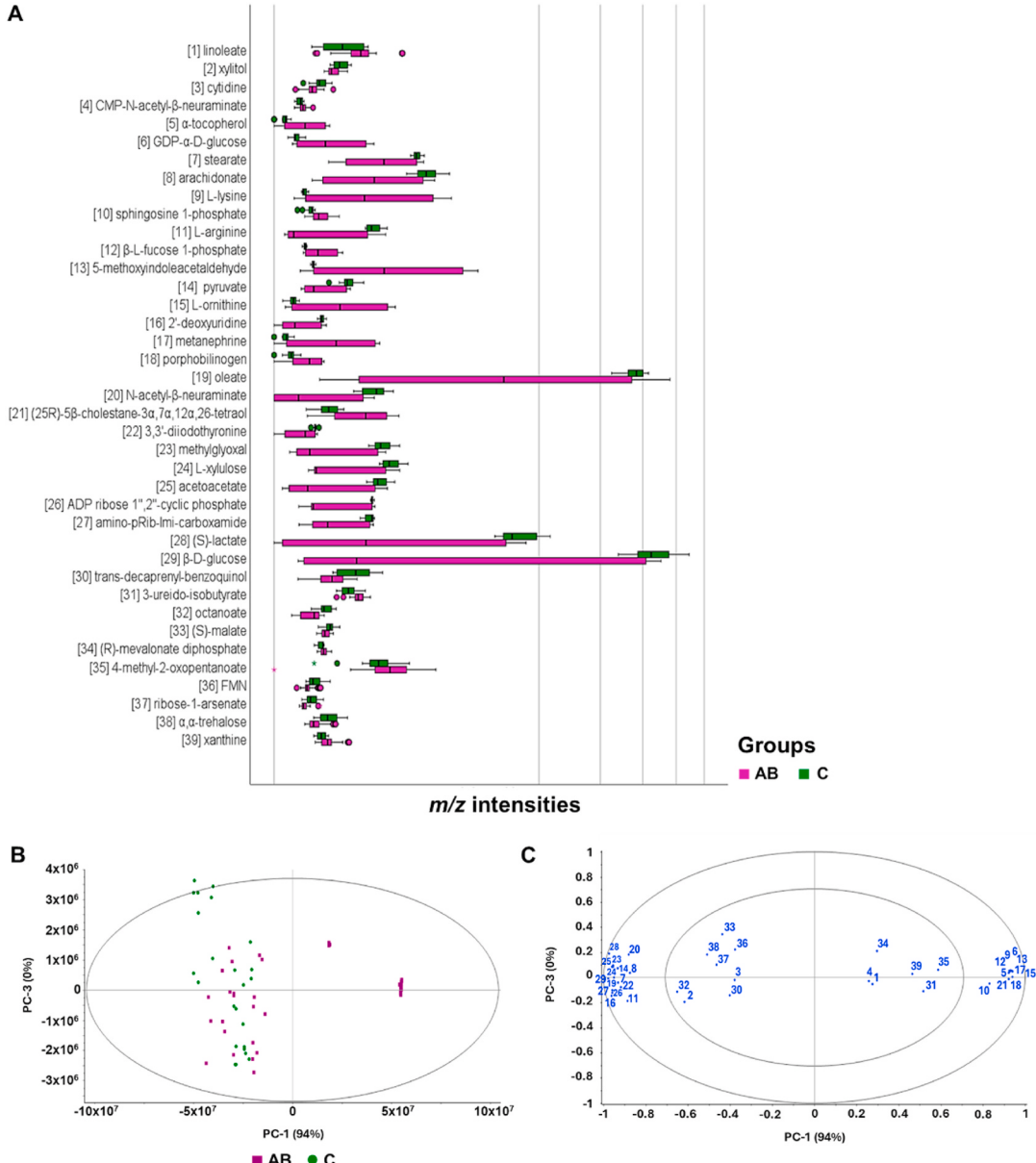


Fig. 3. Impact of mortality on the patients' serum metabolome, based on patients with and without IMV. A: Intensities of the 39 statistically different metabolites between discharged and deceased patients (Group A plus B against C, respectively) ($p < 0.01$), detected by UHPLC-HRMS. The X axis was scaled to the power of 0.3 for better visualization of the boxplots. B: PCA from the 39 metabolites. C: Correlation loadings from both PC1 and PC3, with numbers corresponding to the metabolites listed in panel A. Exterior and interior ellipse corresponds to 100 % and 50 % explained variance, respectively. Abbreviations: amino-pRib-Imi-carboxamide – 5-amino-1-(5-phospho-D-ribosyl)imidazole-4-carboxamide; trans-decaprenyl-benzoquinol – 6-methoxy-3-methyl-2-all-trans-decaprenyl-1,4-benzoquinol.

different sets of metabolites, to quantitatively predict the patients' group (**Table 3**). For each group comparison, seven models were developed, that included the following sets of metabolites: the ones identified as most significantly different between groups as represented on **Fig. 1A**, **2A** and **3A**, respectively, and from these, sub-sets, including the ones highlighted by the corresponding PCA loading vector (**Fig. 1C**, **2C**, **3C**), the ones with the lowest *p*-values and with the highest fold-changes between groups (**Tables S2** and **S3** and **S4**). To conduct a preliminary evaluation of the impact of these sub-sets of metabolites, new PCAs were also performed (**Fig. S1**).

For the comparison between Groups A and B, the best predictive model was based on 13 metabolites with the lowest *p*-value (set number 5 in **Table 3** and **Fig. S1**), that outperformed the model based on 28 metabolites, leading to 100 % sensitivity and specificity for the test data

set. The set of 13 metabolites includes ascorbate and xylitol (carbohydrates), arachidonate (a lipid), N⁴-(*β*-N-acetyl-D-glucosaminyl)-L-asparagine and urocanate (amino acids and derivatives), octanoate, fumarate, and thiamin (involved in energy metabolism), methyloxopentanoate, methyl-2-oxopentanoate, and ureido-isobutyrate (general metabolic intermediates) and bilirubin and urate (excretory end products). The PCA score plot based on these 13 metabolites (**Figs. S1 and A** vs B, set 5) did not show increased separation between the two patient groups. This highlights the relevance of the supervised classification models like compared to non-supervised methods such as PCA.

Regarding the comparison between Groups B and C, the best predictive model was based on eight metabolites (set number 4, **Table 3**), that also outperformed the model based on the original 39 metabolites (**Fig. 2A**), leading to 79 % and 88 % of sensitivity and specificity in

Table 3
PCA or PCA-LDA models' performance based on different set of metabolites to predict patients' group.

Models' Performance	Group A vs B		Group B vs C		Group A+B vs C		
	Calibration	Validation	Calibration	Validation	Calibration	Validation	
	Metabolites n = 28 (<i>p</i> < 0.001)		n = 39 (<i>p</i> < 0.05)		n = 39 (<i>p</i> < 0.01)		
Set 1 - All	Accuracy	98%	92%	91%	69%	84%	
	Sensitivity	96%	100%	85%	63%	82%	
	Specificity	100%	83%	97%	75%	85%	
	Precision	100%	88%	97%	77%	75%	
Set 2 - According to PCA loadings	Metabolites	acetamidobutanal; lactate; glucose; pyridylacetate; <i>myo</i> -inositol (n=5)		dephospho-CoA; pyridyl-butanoate; coumarate; 6-methoxy-3-methyl-2-all-trans-decaprenyl-1,4-benzoquinol; stearate (n=5)		lactate; amino-1-(5-phospho-D-ribosyl) imidazole-4-carboxamide; ADP ribose-1",2"-cyclic-phosphate; acetoacetate; xylulose; methylglyoxal; diiodothyronine; (25R)-5 β -cholestane-3 α ,7 α ,12 α ,26-tetraol; oleate; N-acetyl- β -neuraminate; GDP- α -D-glucose; porphobilinogen; fucose-1-phosphate; metanephrine; methoxyindoleacetaldehyde; deoxyuridine; ornithine; pyruvate; arginine, sphingosine 1-phosphate; arachidonate; lysine; stearate; tocopherol; glucose (n=25)	
	Accuracy	98%	85%	90%	75%	84%	
	Sensitivity	100%	92%	88%	71%	79%	
	Specificity	96%	79%	93%	79%	87%	
	Precision	96%	82%	93%	79%	77%	
Set 3 - Lowest <i>p</i> -values	Metabolites	octanoate; fumarate; methyloxopentanoate (n=3)		4-(3-pyridyl)-butanoate; phenylacetate (n=2)		glucose; lactate; 5-amino-1-(5-phospho-D-ribosyl)imidazole-4-carboxamide; ADP ribose 1",2"-cyclic phosphate (n=4)	
	Accuracy	97%	85%	85%	73%	75%	
	Sensitivity	96%	88%	83%	71%	65%	
	Specificity	97%	83%	88%	75%	79%	
	Precision	97%	84%	87%	77%	62%	
Set 4 - Lowest <i>p</i> -values	Metabolites	Set3 + ureido-isobutyrate; xylitol (n=5)		Set3 + 5,6-dihydouracil; stearate; linoleate; octanoate; CMP-N-acetyl- β -neuraminate; 6-methoxy-3-methyl-2-all-trans-decaprenyl-1,4-benzoquinol (n=8)		glucose; lactate; 5-amino-1-(5-phospho-D-ribosyl)imidazole-4-carboxamide; ADP ribose 1",2"-cyclic phosphate (n=4)	
	Accuracy	97%	75%	97%	83%	85%	
	Sensitivity	96%	71%	97%	79%	74%	
	Specificity	99%	79%	96%	88%	91%	
	Precision	99%	80%	96%	89%	81%	
Set 5 - Lowest <i>p</i> -values	Metabolites	Set4 + urate; ascorbate; methyl-2-oxopentanoate; bilirubin; N ⁴ -(<i>β</i> -N-acetyl-D-glucosaminyl)-L-asparagine; arachidonate; thiamin; urocanate (n=13)		Set 4 + pyruvate; dephospho-CoA; N-acetyl- β -neuraminate; α , α -trehalose; coumarate; lactate; 3-ureido-isobutyrate; 3-pyridylacetate; 4-fumarylacetate; 4-hydroxy-4-(3-pyridyl)-butanoate (n=18)		Set4 + porphobilinogen; metanephrine; deoxyuridine; ornithine; arachidonate; pyruvate; methoxyindoleacetaldehyde; fucose 1-phosphate; acetoacetate; 4-hydroxy-4-(3-pyridyl)-butanoate (n=25)	
	Accuracy	100%	100%	100%	69%	84%	
	Sensitivity	100%	100%	100%	63%	79%	
	Specificity	100%	100%	100%	75%	87%	
	Precision	100%	100%	100%	NA	77%	
Set 6 - Lowest <i>p</i> -values	Metabolites	Set5 + methoxytryptophol; N-acetyl- β -neuraminate; 4-acetamidobutanal; calcitriol; adenosyl-L-homocysteine; 1-pyrroline-3-hydroxy-5-carboxylate; dihydrothymine; dihydrothymine (n=21)		Set5 + FMN; succinate semialdehyde; dihydrothymine; docosahexaenoate (n=22)		Set5 + octanoate; 3-ureido-isobutyrate (n=27)	
	Accuracy	99%	94%	97%	77%	84%	
	Sensitivity	97%	88%	94%	71%	78%	
	Specificity	100%	100%	99%	83%	87%	
	Precision	100%	100%	99%	66%	77%	
Set 7 - Highest fold-change (FC)	Metabolites	acetyl- β -neuraminate; thiamin; gulonate (FC>5; n=3)		4-oxo-4-(3-pyridyl)-butanoate; succinate; inosine; dephospho-CoA; pyridylacetate; dihydrothymine; semialdehyde; 6-methoxy-3-methyl-2-all-trans-decaprenyl-1,4-benzoquinol (FC>2; n=7)		metanephrine; (25R)-5 β -cholestane-3 α ,7 α ,12 α ,26-tetraol; ornithine; lysine; Methoxyindoleacetaldehyde; tocopherol; GDP- α -D-glucose; porphobilinogen; N-acetyl- β -neuraminate; fucose 1-phosphate (FC>3; n=10)	
	Accuracy	92%	83%	97%	77%	80%	
	Sensitivity	85%	67%	94%	63%	63%	
	Specificity	100%	100%	99%	92%	89%	
	Precision	100%	100%	99%	90%	74%	

predicting death, respectively. This model is composed by 4-(3-pyridyl)-butanoate, phenylacetate, 5,6-dihydrouracil, stearate, linoleate, octanoate, CMP-N-acetyl- β -neuraminate, and 6-methoxy-3-methyl-2-all-trans-decaprenyl-1,4-benzoquinol. The PCA for Group B vs C did not show better visual separation compared to the original metabolite set of 39 metabolites (Fig. S1, set 4).

3.3. UHPLC-HRMS: metabolic interpretation

Based on mass spectrometry untargeted analysis, diverse metabolites were highlighted as significantly different between groups. These differences were also observed by others as pointed in the following subsections.

3.3.1. Group a versus group B

The 13 metabolites highlighted by the best predictive model (set 5 in Table 3 and Fig. S1) were also observed in other deregulated processes. The elevated levels of ascorbate, xylitol, and thiamine in ventilated patients (Group B), could have resulted from the parenteral nutrition administered to patients under IMV. The increased levels of xylitol were also previously associated with inflammation, infection and hepatorenal failure [59,60].

Ventilated patients presented increased levels of N⁴-(β -N-acetyl-D-glucosaminyl)-L-asparagine, a metabolite linked to the asparagine degradation pathway [61–63], suggesting altered protein turnover. In contrast, ventilated patients showed lower levels urocanate and 4-methyl-2-oxopentanoate, intermediates in the degradation pathways of histidine and leucine, respectively. Lower levels of urocanate were also observed in infected patients compared to those recovering from COVID-19 [64], and decreased 4-methyl-2-oxopentanoate levels were observed in deceased patients with acute heart failure [65], possibly indicating cardiovascular failure in sepsis [66].

Octanoate levels were elevated in ventilated patients. This metabolite serves as the primary endogenous substrate for lipoic acid in lipoate biosynthesis, which plays protective roles in ischemic events, coagulopathies, and endothelial disorders caused by COVID-19 [67,68]. Higher octanoate serum levels could be indicative of lipoate synthesis blockade, potentially leading to worse outcomes. This increase could also be linked to the inhibition of fatty acid oxidation pathways, as suggested by the decreased levels of arachidonic acid. Lower levels of this omega-6 polyunsaturated fatty acid (PUFA) have been correlated with disease severity and higher mortality rates [69–71]. The lower levels of lipids such as the arachidonic acid can also disrupted lipid signaling pathways crucial for handling inflammation.

Among the 28 metabolites that differed between Groups A and B, notable up-regulations were observed in metabolites associated with energy metabolism in ventilated patients. These include myo-inositol, α -D-glucose, and lactate, which are also elevated in patients with inflammatory conditions [72], septic shock [73], and increased mortality [74]. The up-regulation of these metabolites suggests an enhanced glycolytic flux leading towards an anaerobic metabolism, supported by the downregulation of fumarate, an intermediate of the tricarboxylic acids (TCA) cycle, indicating potential disruption of mitochondrial energy production.

Increased glucose levels can also lead to the activation of the pentose phosphate pathway to generate NADPH, which serves as a reducing equivalent to counteract oxidative stress, correlating with the elevated levels of the antioxidant ascorbate. Decreased levels of arachidonate, docosahexaenoate and PUFAs further underscore possible lipid metabolism alterations.

Acetamidobutanal, linked to amino acid metabolism and the urea cycle, was also deregulated in conditions like acute coronary disease [75] and non-alcoholic fatty liver disease on murine models [76]. Changes in S-adenosyl-L-homocysteine levels, involved in methylation processes, also suggest variations in protein turnover that could reflect muscle wasting and increased proteolysis in severe illness.

3.3.2. Group B versus group C

Relatively to the best set of metabolites between Group B and Group C, reflecting mortality associated to patients under IMV (set 4 in Table 3 and Fig. S1), deceased patients (Group C) presented higher levels of dihydrouracil, which has been associated to ischemic stroke [77], cancer [78], sepsis and systemic inflammatory response syndrome [79]. Octanoate has been associated to disease severity as previously discussed when comparing Group A and B. Increased levels of 6-methoxy-3-methyl-1,2-all-trans-decaprenyl-1,4-benzoquinol, a CoQ10 precursor, may result from mitochondrial dysfunction and, as previously determined by others, could be employed to assess disease severity and patients' outcome in the ICU [80]. On the other hand, the levels of phenylacetate, CMP-N-acetyl- β -neuraminate, and linoleate were decreased in patients of Group C. Lower levels of phenylacetate in deceased patients may be linked to the diminished metabolic activity of anaerobic indigenous microbiota [81]. The CMP-N-acetyl- β -neuraminate, the active form of sialic acid, has been associated with poor cardiac outcomes [82,83] and mortality associated to nephropathy [84]. The decreased values of the omega-6 essential fatty acid, linoleate, that implies deficiencies in omega-3 and 6 PUFAs, has been associated to an increased risk of severe outcomes in deceased patients [85,86].

It is still worth to highlight other significantly different metabolites between these groups (Fig. 2A–Table S3). Lower stearate was observed by others in trauma-septic patients compared to healthy controls [87], and has been associated to inflammation and metabolic syndrome [88,89]. This saturated fatty acid has also been positively associated with obesity in murine models [90], in agreement with its higher value in Group B, that presented twice the number of obese patients relative to group C. Dephospho-coenzyme A (dephospho-CoA) is a coenzyme A precursor in the cytosolic pantothenate biosynthesis. Elevated serum levels of dephospho-CoA may suggest cell leakage resulting from cellular damage, a characteristic previously observed in patients with greater COVID-19 severity [91], such as those in group C. 3-pyridyl-butanoate contributes to the nicotine degradation pathway within the liver, serving as a precursor to pyridylacetate [92]. It is worth noting that three patients from group C were tobacco or ex-tobacco consumers. Coumarate is primarily obtained through dietary intake and is absorbed throughout the entire gastrointestinal tract, and has been associated with beneficial effects, such as antioxidant, antimicrobial, and antiviral properties. This connection implies that this molecule may be linked to better outcomes as previously evidenced by other authors [93–95], therefore explaining its higher levels in Group B, i.e., patients that recovered and were discharged.

Increased levels of glycolytic intermediates like lactate and pyruvate, combined with elevated ribose-1-arsenate, suggest an enhanced glycolytic flux with simultaneous activation of the pentose phosphate pathway. While this would provide NADPH for combating oxidative stress, the reduced succinate and elevated malate indicate potential mitochondrial dysfunction, leading to inefficient energy production via the TCA cycle. Instead of feeding the TCA cycle, pyruvate can be metabolized through anaerobic pathways towards lactate, and towards ketogenesis - elevated octanoate, a medium-chain fatty acid, alongside reduced stearate and linoleate, suggests impaired fatty acid oxidation. This disruption could lead to a reliance on ketogenesis for energy, evidenced by increased keto acids like 4-fumarylacetate. Patients might experience metabolic acidosis and energy deficits, potentially leading to poorer outcomes if the body cannot efficiently utilize fatty acids for energy.

Also, higher levels of arachidonate and docosahexaenoate, combined with increased N-formylkynurenone (a tryptophan metabolite involved in immune modulation), indicate a hyperactive inflammatory and immune response. This could lead to overproduction of pro-inflammatory cytokines and oxidative stress. While initially beneficial for fighting infections, prolonged hyperactivity of the immune system could result in tissue damage and chronic inflammation, worsening the prognosis.

Interestingly, deceased patients (Group C) exhibited increased

pyridylacetate and decreased 5-methoxyindole acetate, suggesting alterations in neurotransmitter metabolism, particularly serotonin and dopamine pathways.

3.3.3. Group a plus B versus group C

The statistically different metabolites between Groups A and B, versus Group C, reflecting mortality in an heterogeneous population, were also observed deregulated by other authors. Elevated ribose-1-arsenate and nucleotides such as cytidine and 2'-deoxyuridine, again suggest an increased pentose phosphate pathway activity, providing NADPH for antioxidant defenses and ribose-5-phosphate for nucleotide synthesis, supporting DNA repair mechanisms. While this may imply a more robust ability to mitigate cell damage, it also hints towards an increased cell damage.

In addition, reduced α -tocopherol and increased arachidonate and stearate levels suggest an imbalance in antioxidant capacity. Although compensatory lipid mediator production may partially offset this deficiency, an overactive inflammatory response, aimed at fighting oxidative stress, can exacerbate tissue damage and contribute to chronic inflammatory conditions, impacting prognosis.

The increased oxidative status can also be linked to mitochondrial dysfunction, as the increased pyruvate and acetoacetate, coupled with lower (R)-mevalonate diphosphate and xanthine, suggest a compensatory shift to ketogenesis due to mitochondrial dysfunction. This adaptation allows the body to rely more on ketone bodies for energy, albeit

compromising long-term metabolic stability. Prolonged dependence on ketogenesis could lead to metabolic acidosis and energy deficits, adversely impacting prognosis.

An increased dependence on ketone bodies for deriving energy at the brain level can also play a role in the neurochemical changes. Elevated 3,3'-diiodothyronine and reduced metanephrine indicate altered thyroid hormone and catecholamine metabolism. These could affect metabolic rate and stress response mechanisms. Neurotransmitter and hormone imbalances might impact mental health and stress response, leading to a slower recovery and to a poorer prognosis.

3.4. UHPLC-HRMS: disease Signature

A disease signature enrichment was conducted to find metabolic signatures common to other diseases (Fig. 4.). The 28 metabolites originally identified as significant different between Group A and B were used for the analysis, allowing to identify common metabolic signatures to diverse metabolic and congenital disorders, as observed in alcoholism and critical illnesses (major trauma, severe septic shock, cardiogenic shock), at a p-value of 0.1 and an enrichment ratio (e.r.) of 8 (Fig. 4A). Interestingly, using only the sub-set of 13 metabolites from the best predictive model (Table 3), the same top disease signatures were maintained, with an increased significance (Fig. 4B, e.r. of 20, with $p < 0.05$).

The 39 metabolites initially recognized as significantly different

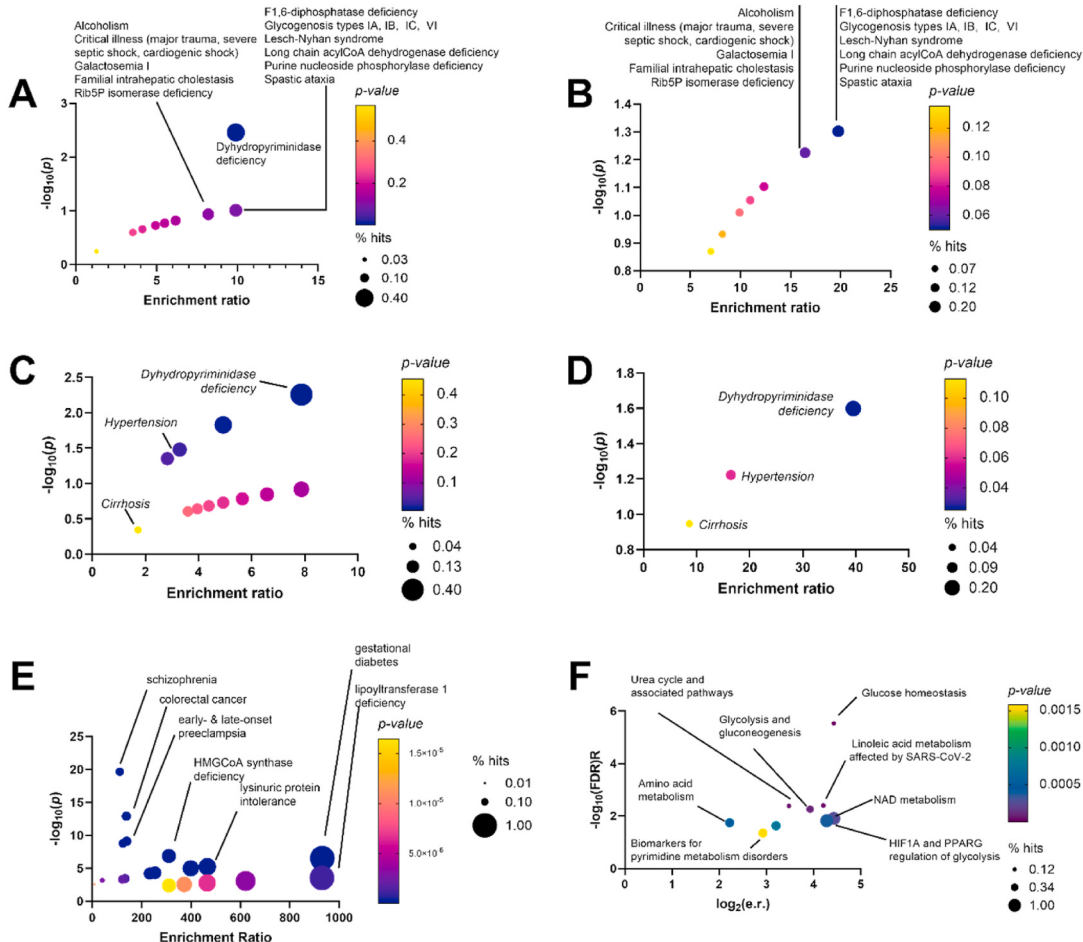


Fig. 4. Disease enrichment based on significantly different metabolites. An enrichment approach was employed to retrieve the global serum changes and identify comparable disease signatures. Enrichment was performed using all the significantly different metabolites between group A and group B patients (A) and between group B and group C patients (C), and also using only the discriminatory metabolites for the group A vs. group B comparison (B) and for the group B vs. group C comparison (D). The disease enrichment using all significantly different metabolites between groups A + B and group C (E) aligns with a large set of different molecular signatures, corresponding to an overrepresentation of a large set of central metabolic pathways (F).

between Group B and C (Fig. 2.), pointed common metabolic signatures as those from dihydropyrimidinase deficiency (e.r. of 7, $p < 0.01$), hypertension (e.r. of 3, $p < 0.05$), and cirrhosis (e.r. of 2, p -value of 0.5) (Fig. 4C). The same correspondence is found when using the sub-set of eight metabolites identified by the best predictive model (Table 3), with increased significance: e.r. of 14, 16, and 9, with p -values below 0.03, 0.05, and of 0.1, for, respectively, dihydropyrimidinase deficiency, hypertension, and cirrhosis (Fig. 4D).

The disease-oriented enrichment analysis, performed with the 39 significantly altered metabolites identified between the Group A and B

versus C (Fig. 3.), matches the molecular signature of many conditions and diseases (Fig. 4E, Table S5), ranging from metabolic deficiencies to cancer-like signatures and CNS-localized conditions, matching the organism-wide symptomatology of COVID. In search of a unifying signature, a second enrichment was performed focusing on the over-represented metabolic pathways. The most significantly over-represented pathways (Fig. 4F), in terms of their biological role, include the sugar turnover and energy production/regulation central pathways, amino acid and protein turnover pathways, once again revealing the systemic effects of COVID at a molecular level.

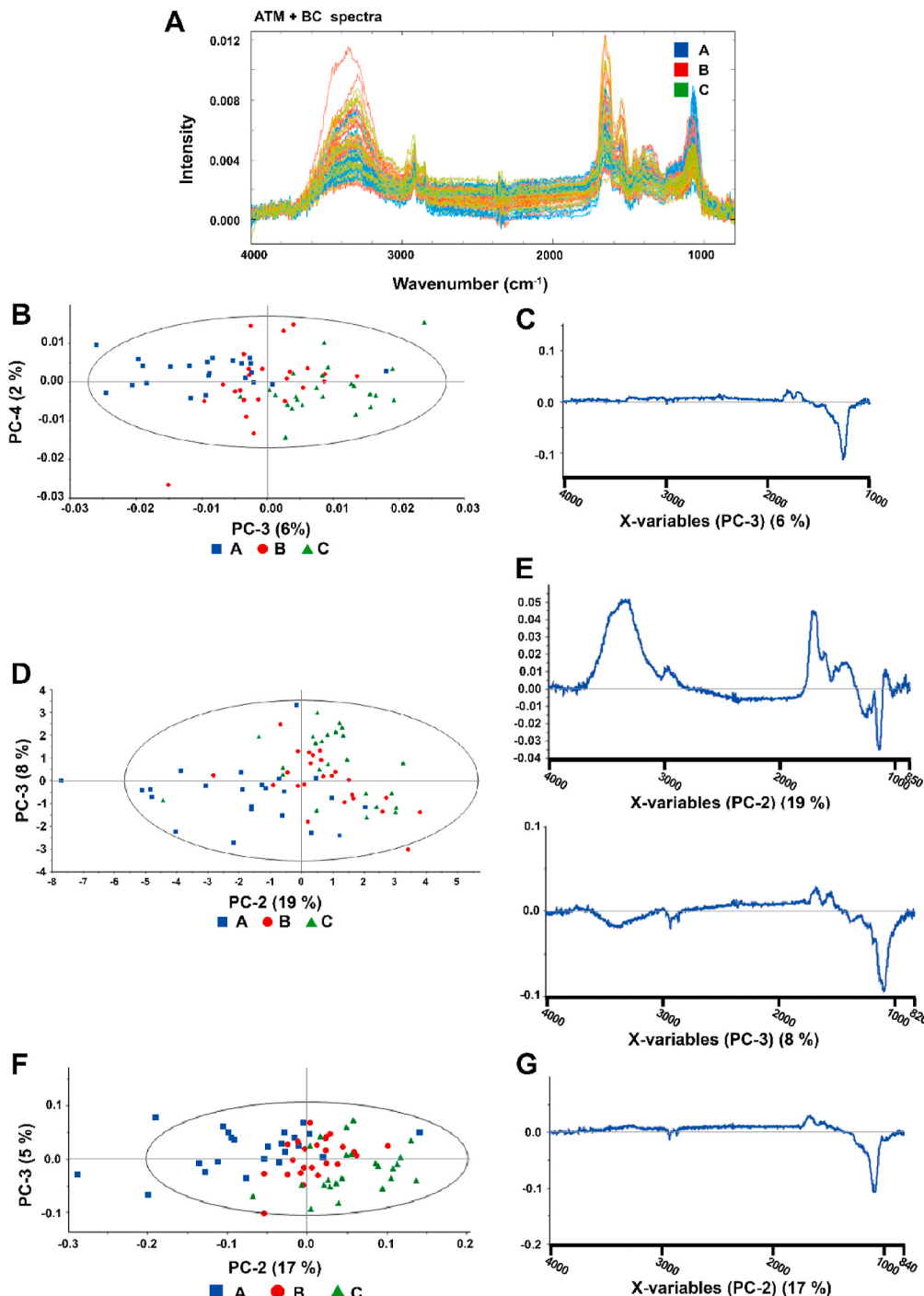


Fig. 5. FTIR spectra of the serum metabolome, from Groups A (blue), B (red) and C (green) (A). Corresponding PCA after atmospheric and baseline corrections (B), atmospheric and baseline corrections with maximum normalization (D), and atmospheric and baseline corrections with unit vector normalization (F). Corresponding PC loadings at the right (C, E and G).

3.5. FTIR-spectroscopy of serum metabolome

FTIR spectral data acquired from serum metabolome samples of 24 patients (Fig. 5A) exhibited low signal-to-noise ratio (SNR), which is consistent with findings from previous work [44]. This was a result from the removal, by precipitation, of the macromolecules with greater impact in the FTIR spectra, such as proteins. Despite the low SNR, the corresponding PCA enabled data clustering according to the patients' groups, i.e., according to the severity of patients' illness (Fig. 5, B, D, F). As observed on the PCAs, less severe patients (without IMV) predominantly cluster on the left side of the plot (Group A in blue). Conversely, patients under IMV are situated on the right side, with deceased patients concentrated on the rightmost side of the plot (Group C in green). This indicates that FTIR spectra captured the molecular fingerprint associated with the illness severity from Group A through C.

Spectra were pre-processed by atmospheric and baseline correction (Fig. 5B), and two normalizations were evaluated, the maximum (Fig. 5D) and the unit vector normalization (Fig. 5F). Normalization increased the explained variance in the two-dimension score-plot from 8 % to 20 %, or higher. This was most probably due to the reduction by normalization of the effect of the samples' concentration, highlighting the differences between their biochemical constituents.

Another interesting observation is that patients with less severe illness (i.e., Group A without IMV) exhibited more dispersed scores in the PCA plot in relation to patients under IMV (Groups B and C), suggesting that the less severe patients presented a more heterogeneous composition of the serum metabolome (Fig. 5F). This is according to the

higher standard deviation observed in the average spectra of Group A, in comparison with the remaining groups (Fig. 6A).

The PC's loadings highlight the spectral regions that contributed most for data clustering in the corresponding score-plot (Fig. 5, C,E,G). Less severe patients (i.e., Group A), presented increased intensities in the wavenumbers 1000-1100 cm⁻¹ (Fig. 5C), due to C-O vibrations from carbohydrates or even C=O vibrations [96]. Patients under IMV (Groups B and C) presented increased intensities in the wavenumbers 1600-1700 cm⁻¹, associated to amide I [97], and 3100-3500 cm⁻¹ related to amides A and B [98].

An inferential statistical analysis focusing bands between 1000 and 1700 cm⁻¹ was subsequently conducted between the three groups (Table 4). Group A exhibited higher intensities across this range, with exception at 1039 cm⁻¹, 1260 cm⁻¹, 1614 cm⁻¹, 1632 cm⁻¹ and 1678 cm⁻¹, where Group B expressed the highest values followed by Group C. For example, Rai et al. [99], observed higher intensities at 1039 cm⁻¹ in a control group compared to patients with oral submucous fibrosis. The wavenumber range 1044–1090 cm⁻¹ showed a significant decreasing trend in values from Group A to Group B to Group C (A > B > C). This range located on the fingerprint region and associated with PO₂⁻ stretching vibration, was also reported by Souza et al. [100] as a significant biomarker region associated to chronic inflammation. The wavenumbers 1102 cm⁻¹ and 1130 cm⁻¹ were significant only in the comparisons between Group A vs B and A + B vs C, both showing a decreasing trend from Group A to B to C. Additionally, the wavenumber 1260 cm⁻¹ was significant only in the Group A vs B comparison. Lacombe et al. [101] linked observed decreasing values of these bands

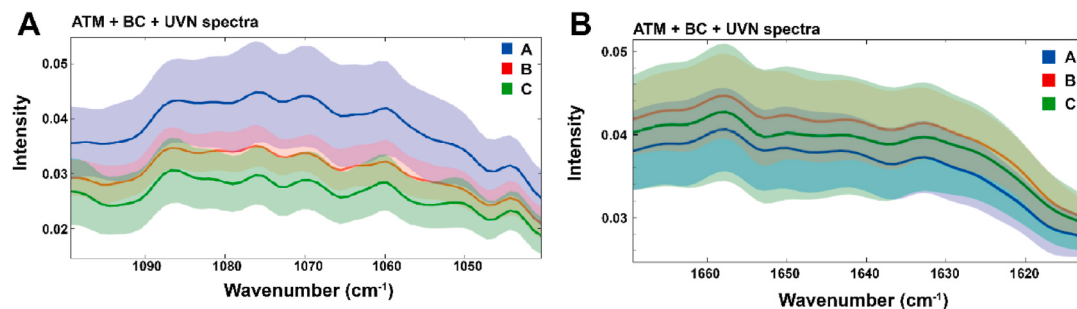


Fig. 6. Average spectra (blue, red and green) and the corresponding standard deviations (shaded) focusing the regions 1000-1100 cm⁻¹ (A), and 1600-1700 cm⁻¹ (B). Spectra was submitted to atmospheric and baseline correction and unit vector normalization. (Group A: blue; Group B: red; Group C: green).

Table 4

Average and standard deviation (s.d.) of absorbance from spectral bands, from spectra pre-processed with atmospheric and baseline correction and unit vector normalization. Statistical analysis was performed using the non-parametric Mann-Whitney U test, with p-values corrected using the Holm-Bonferroni method. p-values <0.05 are highlighted in bold.

Band cm ⁻¹	Group A		Group B		Group C		A vs. B	B vs. C	A & B vs. C
	Average	s.d.	Average	s.d.	Average	s.d.			
1026	0.0183	0.0036	0.0166	0.0028	0.0156	0.0026	0,136	0,421	0,136
1039	0.0183	0.0050	0.0208	0.0031	0.0188	0.0032	0,001	0,039	0,0004
1044	0.0314	0.0056	0.0255	0.0032	0.0232	0.0036	0,00006	0,037	0,0001
1069	0.0441	0.0094	0.0336	0.0035	0.0288	0.0054	3,36E-06	0,001	3,27E-06
1075	0.0441	0.0092	0.0348	0.0038	0.0295	0.0055	0,00001	0,0006	0,000002
1090	0.0388	0.0076	0.0310	0.0035	0.0264	0.0056	0,00003	0,003	0,00002
1102	0.0388	0.0058	0.0277	0.0038	0.0257	0.0062	0,0003	0,112	0,004
1130	0.0248	0.0035	0.0207	0.0020	0.0193	0.0034	0,00007	0,140	0,001
1260	0.0150	0.0020	0.0136	0.0018	0.0134	0.0017	0,028	0,523	0,090
1520	0.0150	0.0021	0.0194	0.0033	0,0190	0.0031	1000	1000	1000
1542	0.0233	0.0022	0.0245	0.0046	0.0237	0.0050	1000	1000	1000
1565	0.0233	0.0019	0.0258	0.0030	0.0252	0.0035	0,605	1000	1000
1614	0.0280	0.0028	0.0306	0.0026	0.0299	0.0038	0,008	0,757	0,686
1632	0.0380	0.0044	0.0413	0.0043	0.0397	0.0066	0,007	0,992	0,992
1644	0.0380	0.0047	0.0416	0.0050	0.0399	0.0075	0,061	1000	1000
1650	0.0406	0.0050	0.0423	0.0054	0.0402	0.0082	0,090	0,819	0,952
1657	0.0406	0.0051	0.0446	0.0052	0.0427	0.0084	0,072	0,796	0,923
1678	0.0353	0.0037	0.0381	0.0032	0.0369	0.0060	0,030	1000	1000

Table 5

Average performance of the calibration (Cal) and validation (Val) of PCA-LDA models based on FTIR spectra of the serum metabolome to predict patients' group. The top-performing models are presented in bold. (Abbreviations: ATM: Atmospheric Correction; BC: Baseline Correction; MAX: Maximum normalization; UVN: Unit Vector Normalization).

Spectra pre-processing	Group A vs Group B		Group B vs Group C		Group A & B vs Group C		
	Cal	Val	Cal	Val	Cal	Val	
ATM + BC	Accuracy	86 %	79 %	76 %	60 %	82 %	83 %
	Sensitivity	87 %	83 %	81 %	63 %	83 %	83 %
	Specificity	86 %	74 %	72 %	58 %	81 %	83 %
	Precision	86 %	77 %	75 %	58 %	69 %	74 %
ATM + BC + UVN	Accuracy	84 %	83 %	74 %	73 %	81 %	71 %
	Sensitivity	86 %	83 %	68 %	67 %	81 %	75 %
	Specificity	81 %	83 %	79 %	79 %	81 %	69 %
	Precision	82 %	85 %	77 %	81 %	69 %	63 %
ATM + BC + MAX	Accuracy	83 %	81 %	74 %	71 %	88 %	76 %
	Sensitivity	86 %	92 %	68 %	71 %	83 %	67 %
	Specificity	80 %	70 %	79 %	71 %	90 %	81 %
	Precision	82 %	77 %	78 %	69 %	82 %	67 %

from healthy to diabetic to galactosemic patients' plasma. This trend reflects increasing metabolic dysregulation from Group A to C, aligning with the UHPLC-HRMS findings, where patients in Groups B and C showed elevated serum levels of lactate and glucose, associated with inflammation and sepsis, as also noted by Lacombe et al. At higher wavenumber bands, significant differences were observed only between Group A and Group B, particularly at 1614 cm^{-1} , 1644 cm^{-1} , and 1678 cm^{-1} , with Group B showing higher values. These wavenumbers are associated with the amide I band [31], and have been implicated in several studies focused on conditions like Parkinson's and Alzheimer's disease [102] and hypothyroidism [103].

In general, good predictive models were developed for all comparisons (see Table 5), with sensitivities and specificities higher than 70 %. For the comparisons between Group A and B, in the validation model a sensitivity and a specificity of 83 % were achieved. For Group B versus C, were obtained models with lower performances, with a sensitivity and a specificity of 71 %. This most probably resulted from the fact that Groups B and C were more homogenous between them, comparatively to Groups A and B, as previously mentioned.

3.6. FTIR-spectroscopy of whole serum

Due to the low SNR of spectra obtained from serum after macromolecule removal, FTIR spectra from the whole serum, i.e., without the precipitation of macromolecules, was also evaluated (Fig. 7). The impact of diverse pre-processing methods, such as baseline correction and two normalizations were evaluated. Due to the significantly higher SNR the spectra second derivative was also assessed, considering the whole spectra or the sub-regions between 800 and 1800 cm^{-1} and 2800 - 3100 cm^{-1} .

PCA-LDA models based on FTIR spectra of whole serum were developed considering diverse spectra pre-processing methods, and the validation process conducted as previously explained, leading to 60 models (Table 6). Reasonable models for the comparison between Groups A and B were obtained. Unexpectedly, and in contrary to the models based on the serum metabolome, it was not possible to develop predictive models for death (Group C), when comparing only with Group A, or when comparing to Groups A plus B. This underscores the importance of the serum metabolome and its biochemical signature, which can be more directly linked to the phenotype of a disease, compared to the whole serum.

4. Discussion

Serum metabolomics can represent a critical platform to discover biomarkers for disease diagnosis and prognosis, including in highly heterogeneous and dynamic populations of critically ill patients at ICUs.

The current work aimed to compare two platforms to capture the groups' metabolic fingerprint, namely UHPLC-HRMS and FTIR spectroscopy. While UHPLC-HRMS offers higher resolution and allows to identify metabolite sets to enhance the understanding of the underlying biochemical mechanisms of diseases, it comes with more complex, time-consuming, and expensive processes compared to the FTIR-spectroscopy-based platform. This last technique, by capturing fundamental molecular vibrations of various functional groups in complex biological samples, can also capture the molecular fingerprint associated with the system's metabolic status. It is rapid, as a spectrum can be acquired in 1 min, and can be used in an automatic high-throughput mode based on microplates with, for example, $5\text{ }\mu\text{L}$ of each sample analysed in plates with 96 or 384 wells, requiring only simple sample dehydration. Consequently, we predict that FTIR spectroscopy analysis is much cheaper (approximately 60 times less expensive), faster (approximately 10 times quicker), and simpler, making it more suitable for large-scale studies.

To compare the two platforms, we considered serum samples from three groups of ICU patients (A, B and C), each with 8 patients. Patients in Groups B and C were on their eighth and ninth day of IMV, respectively. Invasive mechanical ventilation (IMV) can significantly impact the metabolomic profile of ICU patients by altering key metabolic processes such as energy metabolism, amino acid profiles, and lipid metabolism. Prolonged IMV triggers physiological stress, inflammation, and oxidative stress, which influence the serum metabolite landscape. These shifts, often seen in critical illness, lead to changes in metabolites related to glucose, lipids, and proteins [104].

Group C died a median of five days after the current analysis. In this context, while early-phase biomarkers capture acute inflammatory or traumatic responses, our study aimed to identify subacute biomarkers emerging during the 5th to 7th days of ICU admission. This subacute phase is marked by critical physiological changes that are more closely linked to long-term outcomes and the efficacy of interventions. By focusing on this window, our objective was to uncover biomarkers that could better predict recovery or deterioration, providing valuable insights for improving clinical decision-making in critically ill COVID-19 patients [105,106]. Due to the patients' characteristics and limited group dimensions (Table 1), the developed predictive models present inherent limitations. This is especially relevant for critically ill patients admitted to ICUs, that present a high variety of comorbidities, and very dynamic changes in their clinical status and medication. Due to all these limitations, it is relevant to employ platforms that can be implemented in simple and high-throughput modes, in large-scale populations. This was the major goal of the present work, not so to develop robust predictive models, but to compare two significantly different platforms concerning their outputs.

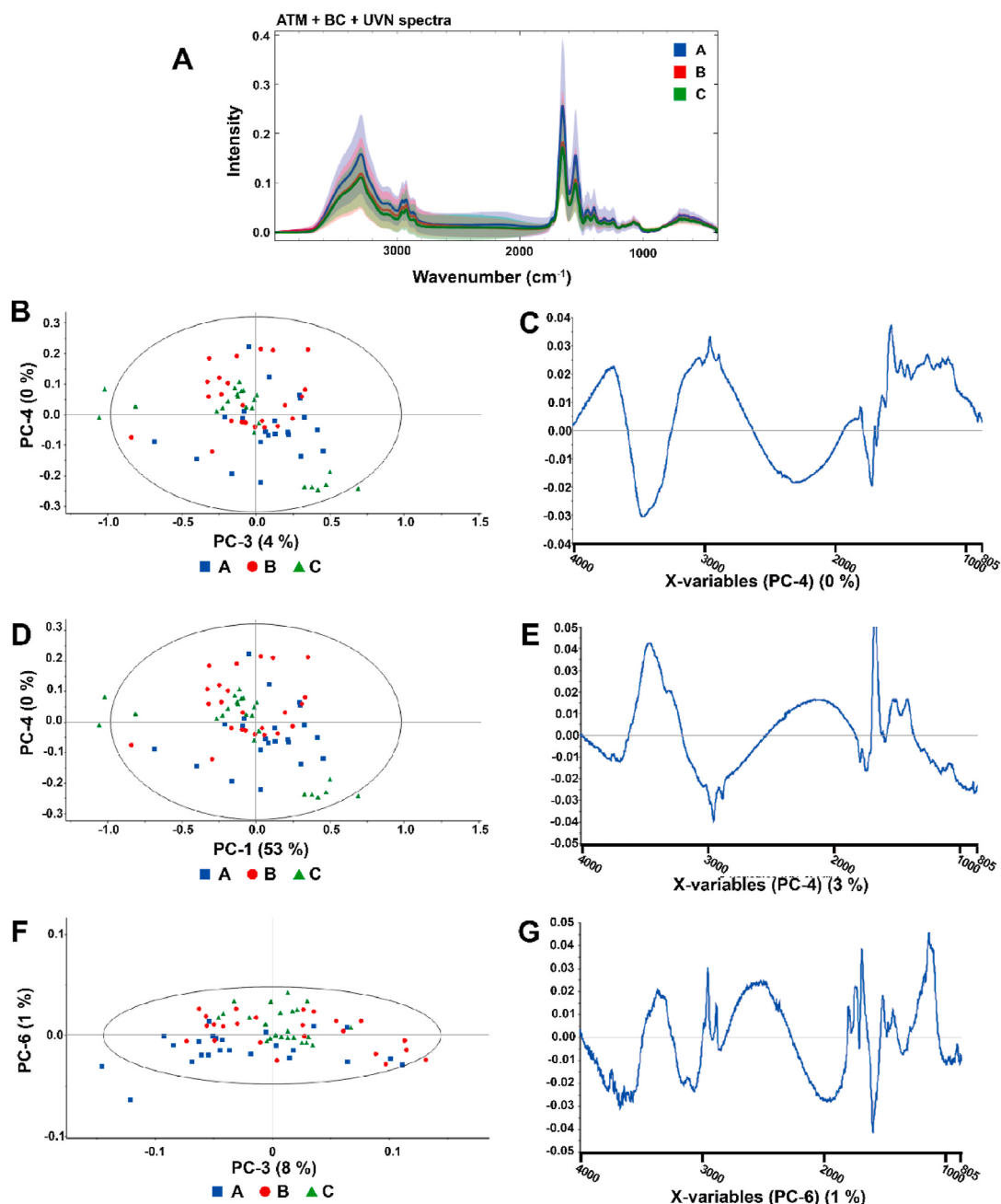


Fig. 7. Average FTIR spectra (line in blue, red and green) and the corresponding standard deviations (shaded blue, red and green) of whole serum of patients from Group A (blue), B (red) and C(green) (A). Corresponding PCA after atmospheric and baseline corrections (B), atmospheric and baseline corrections with maximum normalization (D), and atmospheric and baseline corrections with unit vector normalization (F). Respective PC loadings at the right (C)(E)(G).

4.1. The UHPLC-HRMS based-platform

An advantage of UHPLC-HRMS is its theoretical high resolution in identifying molecular features. Using both RP and HILIC columns and conducting analyses in both positive and negative ionization modes, UHPLC-HRMS yielded approximately 23,000 m/z peaks per group, with about half of these peaks isolated from each type of column. This highlights the complementary nature to the two chromatographic setups to increase metabolite coverage, since HILIC detects mostly polar molecules, while RP separation focuses on non to mid polar compounds [107]. Furthermore, out of the 13 metabolites used in the best predictive model for comparing Group A with B, seven were identified by both RP and HILIC columns, one was exclusively isolated by the RP column, and five were isolated by the HILIC column. Regarding the best model when

comparing Group B to C, three metabolites were identified by the RP column and five by the HILIC column. All this highlights the relevance of using the two chromatographic systems to increase metabolite coverage. These findings highlight the complementary strengths of HILIC and RP columns in metabolite detection. While the HILIC column excels in identifying a greater number of relevant metabolites for our study, the RP column significantly contributes by detecting metabolites that are exclusive to its methodology. Specifically, the RP column identified 38 % of the metabolites used in the best discriminating model for distinguishing Groups B and C, underscoring its importance. Furthermore, when examining the other significantly different metabolites between Groups A and B, B and C, and A and B versus C, it is evident that a substantial proportion were detected primarily by HILIC. This reinforces the necessity of employing both chromatographic approaches in future

Table 6

Average performance of the calibration (Cal) and validation (Val) of PCA-LDA models, based on FTIR spectra of whole serum, to predict patients' group. The best-performing models are highlighted in bold. (Abbreviations: ATM: Atmospheric Correction; BC: Baseline Correction; MAX: Maximum normalization; UVN: Unit Vector Normalization; 2nd Deriv.: second derivative transformation).

Spectra pre-processing	Group A vs Group B		Group B vs Group C		Group A & B vs Group C	
	Cal	Val	Cal	Val	Cal	Val
ATM + BC	Accuracy	80 %	65 %	67 %	33 %	79 %
	Sensitivity	76 %	58 %	72 %	50 %	58 %
	Specificity	83 %	71 %	61 %	17 %	90 %
	Precision	82 %	67 %	65 %	37 %	75 %
ATM + BC + UVN	Accuracy	80 %	58 %	69 %	52 %	81 %
	Sensitivity	74 %	54 %	65 %	46 %	68 %
	Specificity	86 %	63 %	74 %	58 %	87 %
	Precision	85 %	63 %	72 %	41 %	73 %
ATM + BC + MAX	Accuracy	83 %	71 %	71 %	38 %	81 %
	Sensitivity	81 %	75 %	72 %	58 %	72 %
	Specificity	86 %	67 %	69 %	17 %	86 %
	Precision	85 %	68 %	72 %	40 %	73 %
ATM+2nd Deriv.	Accuracy	88 %	63 %	80 %	25 %	70 %
	Sensitivity	92 %	75 %	78 %	29 %	28 %
	Specificity	85 %	50 %	82 %	21 %	92 %
	Precision	86 %	70 %	81 %	27 %	NA
ATM+2nd Deriv. 800-1800 cm ⁻¹ and 2800-3100 cm ⁻¹	Accuracy	94 %	79 %	83 %	27 %	82 %
	Sensitivity	96 %	79 %	83 %	25 %	65 %
	Specificity	92 %	79 %	82 %	29 %	90 %
	Precision	93 %	86 %	83 %	NA	79 %

studies to achieve a more comprehensive understanding of the metabolomic landscape.

While moving from a univariate approach to a LDA or PCA-LDA sustained approach, it was possible to define a low number of discriminatory metabolites (13 when comparing A vs. B, and eight when comparing B vs. C), in relation to the number based on univariate data analysis (28 when comparing A vs. B, and 39 when comparing B vs. C). This smaller set of metabolites represented the different biological signatures between patient groups, while also increasing the performances of the predictive models and the significance of the top disease signatures obtained by the disease enrichment analysis. All these points indicate that the process implemented in the present work to discover sets of metabolites for predicting disease status and outcomes has successfully identified metabolic signatures that are most likely in line with the clinical scenario.

It was possible to develop LDA predictive models based on 13 metabolites, enabling to distinguish patients in Group B (under IMV) from those in Group A (without IMV), with 100 % specificity and sensitivity. Among all patients under IMV (Groups B and C), it was possible to predict death (Group C) based on eight metabolites, with a specificity of 79 % and a sensitivity of 88 %. The lower performance of this predictive model most probably reflects the more homogenous characteristics among patients in Groups B and C, who were all under IMV.

However, it was not possible to develop predictive models for patients' death (Group C) based on sets of metabolites when a more heterogeneous population was considered, i.e., patients in the control group with and without IMV (Groups A and B together).

In disease enrichment analysis for both Group A vs B and Group B vs C, the disease signatures obtained from filtering the original metabolite sets (28 and 39, respectively) to the sets retrieved from the best predictive models not only maintained the same disease signature but also increased their statistical significance. This highlights the relevance of the method used to optimize the predictive models. Interestingly, Group B had twice as many patients with hypertension compared to Group C. The fact that the metabolomic signature of critically ill patients with COVID-19 resembles that of cirrhosis can be explained by the system-wide immunological activation triggered by the virus [108,109]. Similarly, COVID-19 is also associated with the onset of new high blood pressure [110], as identified through the enrichment analysis.

4.2. The FTIR-spectroscopy based-platform

The FTIR-spectra of the serum metabolome enabled the development of good predictive models for group comparisons A vs. B (accuracy 83 %), and B vs. C (accuracy 71 %). These models, though with lower performances than those from the previous platform (with accuracies of 100 % and 83 %, respectively), offer significant advantages. FTIR-based models are derived from analyses that can be performed in a simple, economic, and high-throughput mode, making them more suitable for large-scale studies.

Furthermore, this platform enabled to develop a predictive model for death in the ICU (Group C), when considering a more heterogeneous control group (patients from Groups A and B), with a sensitivity and specificity for the validation set of 83 %. This was a very promising and unexpected result since it was not possible to develop predictive models for death based on sets of defined metabolites.

Despite not identifying defined metabolites, the sensitivity of FTIR spectroscopy in acquiring the metabolic status of the system is highlighted. This sensitivity was also pointed by the higher dispersion of scores Group A patients, emphasizing the more heterogeneous composition of these patients' serum (Fig. 5). This contrasts the more homogeneous serum molecular composition of patients from Groups B and C, both commonly under an artificial gastric feeding and the IMV procedure (Fig. 5). This was also highlighted by the higher standard deviation observed in the average spectra of Group A, in comparison to the remaining groups (Fig. 6A), and the higher standard deviations associated to spectral bands (Table 4). Furthermore, FTIR spectra indicated an increase in spectral bands associated with amide groups with illness severity (Fig. 5), consistent with the heightened inflammatory states detected by the UHPLC-HRMS platform.

Interestingly, it was possible to develop slightly better models when evaluating the impact of IMV, based on the FTIR spectra of the serum metabolome (accuracy 83 %), despite the lower SNR spectral data, when compared with the FTIR spectra of whole serum analysis (accuracy 79 %). Furthermore, it was not possible to develop predictive models for death, based on the FTIR spectral of the whole serum. This underscores the importance of the serum metabolome and its biochemical signature, which can be more directly linked to the phenotype of a disease, compared to the whole serum.

5. Conclusions

When comparing two analytical platforms to acquire the molecular fingerprint associated to the serum metabolome of critically ill patients at a general ICU, the UHPLC-HRMS enabled to develop good to excellent predictive models, when considering balanced populations between the control and study groups, with increased performances (e.g. with 8 %–17 % higher accuracies) in relation to FTIR-spectroscopy. Another advantage of the UHPLC-HRMS platform, is that the discovered set of metabolites can potentiate a better understanding of complex pathophysiological processes, and consequently to discover new therapeutic approaches. However, all this was not possible to achieve when considering unbalanced populations, where the FTIR-spectroscopic based platform, enabled to develop good predictive models, with the supplementary advantages over the UHPLC-HRMS system, of the FTIR spectra being acquired in simple, rapid, economic and high-throughput modes, more easily implemented to large scale populations, and consequently leading to predictive models more easily translatable to the clinical environment. Therefore, FTIR-spectroscopy based platforms is an attractive complementary method to capture the system metabolic fingerprint, to discover biomarkers of diseases status and diseases outcome.

The UHPLC-HRMS demonstrated superior performance in generating predictive models for groups with balanced characteristics, achieving accuracies of 83 % or higher. This platform's ability to provide detailed metabolite profiles underpins its robustness and potential for identifying specific biomarkers linked to the severity of illness and mortality in critically ill patients. In contrast, FTIR spectroscopy excelled in the context of unbalanced groups, particularly in the combined analysis of Groups A and B versus Group C. Its simplicity, cost-effectiveness, and rapid processing capability make it an attractive option for large-scale studies and clinical applications where rapid decision-making is essential. The high-throughput nature of FTIR spectroscopy also supports its use in settings with diverse patient populations, addressing the need for broader applicability in clinical environments.

Clinically, these findings suggest that while UHPLC-HRMS can contribute significantly to personalized medicine by providing comprehensive metabolomic data, FTIR spectroscopy offers a practical alternative for quick assessments, potentially guiding initial clinical decisions and stratifying patients based on risk.

The metabolites identified through these analyses shed light on the underlying metabolic disturbances in patients requiring IMV. Understanding these pathways could lead to new therapeutic approaches, particularly in modulating metabolic responses to improve outcomes.

However, the study faced several limitations, including a relatively small sample size and the heterogeneity of ICU populations, which may affect the generalizability of the findings. Additionally, the integration of metabolomics into clinical practice poses challenges due to the technical complexity and cost of platforms like UHPLC-HRMS, favoring a more straightforward alternative like FTIR spectroscopy.

Future research should focus on larger cohort studies to validate these findings and explore the integration of metabolomics with other omics technologies to enhance our understanding of the complex interplay of factors influencing critical illness. Advances in machine learning and analytical techniques could further improve the predictive power and clinical utility of these metabolomics platforms.

CRediT authorship contribution statement

Tiago A.H. Fonseca: Writing – review & editing, Writing – original draft, Methodology, Formal analysis, Conceptualization. **Cristiana P. Von Rekowski:** Writing – review & editing, Writing – original draft, Formal analysis. **Rúben Araújo:** Writing – review & editing, Formal analysis. **M. Conceição Oliveira:** Writing – review & editing, Methodology. **Gonçalo C. Justino:** Writing – review & editing, Writing –

original draft, Methodology, Formal analysis, Conceptualization. **Luís Bento:** Writing – review & editing, Methodology. **Cecília R.C. Calado:** Writing – review & editing, Writing – original draft, Methodology, Formal analysis, Conceptualization.

Informed consent statement

Informed consent was obtained from all subjects involved in the study.

Institutional review board statement \ ethical approval

The study was conducted in accordance with the Declaration of Helsinki and approved by the Institutional CHULC Ethics Committee (1043/2021, 20/05/2020).

Consent for publication

Not applicable.

Availability of data and materials

The datasets generated and/or analysed during the current study are not publicly available due to General Data Protection Regulation but are available from the corresponding author on reasonable request.

Funding

This research was funded by Fundação para a Ciência e a Tecnologia (FCT), grant numbers DSAIPA/DS/0117/2020 and RNEM-LISBOA-01-0145-FEDER-022125 (Portuguese Mass Spectrometry Network). Centro de Química Estrutural is a Research Unit funded by FCT through projects UIDB/00100/2020 and UIDP/00100/2020. Institute of Molecular Sciences is an Associate Laboratory funded by FCT through project LA/P/0056/2020.

Declaration of competing interest

The authors declare that they have no known competing financial interests or personal relationships that could have appeared to influence the work reported in this paper.

Acknowledgments

Not applicable.

Appendix A. Supplementary data

Supplementary data to this article can be found online at <https://doi.org/10.1016/j.combiomed.2024.109393>.

References

- [1] D.S. Wishart, Metabolomics for investigating physiological and pathophysiological processes, *Physiol. Rev.* 99 (4) (Oct. 2019) 1819–1875, <https://doi.org/10.1152/physrev.00035.2018>.
- [2] R. Araújo, L.F.N. Bento, T.A.H. Fonseca, C.P. Von Rekowski, B.R. da Cunha, C.R. C. Calado, Infection biomarkers based on metabolomics, *Metabolites* 12 (2) (Jan. 2022) 92, <https://doi.org/10.3390/metabo12020092>.
- [3] C.H. Johnson, F.J. Gonzalez, Challenges and Opportunities of Metabolomics, John Wiley & Sons, Ltd, Aug. 01, 2012, <https://doi.org/10.1002/jcp.24002>.
- [4] K. Huang, N. Thomas, P.R. Gooley, C.W. Armstrong, Systematic review of NMR-based metabolomics practices in human disease research, *Metabolites* 12 (10) (2022), <https://doi.org/10.3390/metabo12100963>.
- [5] B.C. Muthubharathi, T. Gowripriya, K. Balamurugan, Metabolomics: small molecules that matter more, *Mol. Omi.* 17 (2) (2021) 210–229, <https://doi.org/10.1039/d0mo00176g>.
- [6] T. Vanden Berghe, E. Hoste, Paving the Way for Precision Medicine v2.0 in Intensive Care by Profiling Necroinflammation in Biofluids, vol. 10, Nature Publishing Group, 2019, <https://doi.org/10.1038/s41418-018-0196-2>. Jan.

- [7] R. Powers, E. Riekeberg, New frontiers in metabolomics: from measurement to insight, *F1000Research* 6 (0) (2017), <https://doi.org/10.12688/f1000research.11495.1>.
- [8] A.V. Aderemi, A.O. Ayeloso, O.O. Oyedapo, E. Mukwewho, Metabolomics: a scoping review of its role as a tool for disease biomarker discovery in selected non-communicable diseases, *Metabolites* 11 (7) (2021), <https://doi.org/10.3390/metabo11070418>.
- [9] S. Moco, J.M. Buescher, Metabolomics: going deeper, going broader, going further, *Methods Mol. Biol.* 2554 (2023) 155–178, https://doi.org/10.1007/978-1-0716-2624-5_11. *Methods Mol Biol.*
- [10] P.A. LeWitt, J. Li, M. Lu, L. Guo, P. Auinger, Metabolomic biomarkers as strong correlates of Parkinson disease progression, *Neurology* 88 (9) (Feb. 2017) 862–869, <https://doi.org/10.1212/WNL.00000000000003663>.
- [11] C. Martins, S. Magalhães, I. Almeida, V. Neto, S. Rebelo, A. Nunes, Metabolomics to study human aging: a review, *Curr. Mol. Med.* 23 (Apr) (2023), <https://doi.org/10.2174/156562402366230407123727>.
- [12] P. Di Carlo, et al., A systematic review on omics data (metagenomics, metatranscriptomics, and metabolomics) in the role of microbiome in gallbladder disease, *Front. Physiol.* 13 (August) (Aug. 2022) 1–14, <https://doi.org/10.3389/fphys.2022.888233>.
- [13] A.G. Mukherjee, et al., Recent advances in understanding brain cancer metabolomics: a review, *Med. Oncol.* 40 (8) (Jul. 2023) 220, <https://doi.org/10.1007/s12032-023-02109-3>.
- [14] R. Subramani, S. Poudev, K.D. Smith, A. Estrada, R. Lakshmanaswamy, Metabolomics of breast cancer: a review, *Metabolites* 12 (7) (Jul. 2022) 643, <https://doi.org/10.3390/metabo12070643>.
- [15] L. Guo, H. Jin, Research progress of metabolomics in psoriasis, *Chin. Med. J.* 136 (15) (Aug. 2023) 1805–1816, <https://doi.org/10.1097/CM9.0000000000002504>.
- [16] M. Vacca, et al., How metabolomics provides novel insights on celiac disease and gluten-free Diet: a narrative review, *Front. Microbiol.* 13 (Jun) (2022), <https://doi.org/10.3389/fmicb.2022.859467>.
- [17] L. Xu, et al., Metabolomics in rheumatoid arthritis: advances and review, *Front. Immunol.* 13 (Aug) (2022), <https://doi.org/10.3389/fimmu.2022.961708>.
- [18] A. Hertzog, A. Selvanathan, B. Devanapalli, G. Ho, K. Bhattacharya, A.A. Tolun, A Narrative Review of Metabolomics in the Era of ‘omics’: Integration into Clinical Practice for Inborn Errors of Metabolism, AME Publishing Company, Oct. 01, 2022, <https://doi.org/10.21037/tp-22-105>.
- [19] L.N.F. Guerreiro Costa, et al., Metabolomics of major depressive disorder: a systematic review of clinical studies, *Cureus* 14 (3) (Mar. 2022), <https://doi.org/10.7759/cureus.23009>.
- [20] Z.A. Damanhouri, H.M. Alkreaty, F.A. Alharbi, H. Abualhamail, M.S. Ahmad, A review of the impact of pharmacogenetics and metabolomics on the efficacy of metformin in type 2 diabetes, *Int. J. Med. Sci.* 20 (1) (2023) 142–150, <https://doi.org/10.7150/ijms.77206>.
- [21] V. Pirro, et al., Effects of tirzepatide, a dual GIP and GLP-1 RA, on lipid and metabolite profiles in subjects with type 2 diabetes, *J. Clin. Endocrinol. Metab.* 107 (2) (Jan. 2022) 363–378, <https://doi.org/10.1210/clinend/gdagb722>.
- [22] R. Araújo, L. Ramalhete, E. Ribeiro, C. Calado, Plasma versus serum analysis by FTIR spectroscopy to capture the human physiological state, *Biotechnologia* 11 (4) (Dec. 2022) 56, <https://doi.org/10.3390/biotech11040056>.
- [23] A. Zhang, H. Sun, X. Wang, Serum metabolomics as a novel diagnostic approach for disease: a systematic review, *Anal. Bioanal. Chem.* 404 (4) (Sep. 2012) 1239–1245, <https://doi.org/10.1007/s00216-012-6117-1>.
- [24] O. Kiseleva, I. Kurbatov, E. Ilgisonis, E. Poverennaya, Defining Blood Plasma and Serum Metabolome by Gc-Ms, MDPI, Jan. 01, 2022, <https://doi.org/10.3390/metabol2010015>.
- [25] A. Di Minno, M. Gelzo, M. Caterino, M. Costanzo, M. Ruoppolo, G. Castaldo, Challenges in metabolomics-based tests, biomarkers revealed by metabolomic analysis, and the promise of the application of metabolomics in precision medicine, *Int. J. Mol. Sci.* 23 (9) (May 2022) 5213, <https://doi.org/10.3390/ijms23095213>.
- [26] W.B. Dunn, et al., Procedures for large-scale metabolic profiling of serum and plasma using gas chromatography and liquid chromatography coupled to mass spectrometry, *Nat. Protoc.* 6 (7) (Jul. 2011) 1060–1083, <https://doi.org/10.1038/nprot.2011.335>.
- [27] L. Dossus, et al., Prospective analysis of circulating metabolites and endometrial cancer risk, *Gynecol. Oncol.* 162 (2) (Aug. 2021) 475–481, <https://doi.org/10.1016/j.ygyno.2021.06.001>.
- [28] A. Tripp, G. Poulogiannis, Banking on metabolomics for novel therapies in TNBC, *Cell Res.* 32 (5) (Feb. 2022) 423–424, <https://doi.org/10.1038/s41422-022-00637-7>.
- [29] Y. Chen, E.M. Li, L.Y. Xu, Guide to Metabolomics Analysis: A Bioinformatics Workflow, vol. 15, 2022, <https://doi.org/10.3390/metabo12040357>, Apr.
- [30] L.M. Ramalhete, R. Araújo, A. Ferreira, C.R.C. Calado, Proteomics for biomarker discovery for diagnosis and prognosis of kidney transplantation rejection, *Proteomes* 10 (3) (Jul. 2022) 24, <https://doi.org/10.3390/proteomes10030024>.
- [31] Z. Movasaghi, S. Rehman, D.I. ur Rehman, Fourier transform infrared (FTIR) spectroscopy of biological tissues, *Appl. Spectrosc. Rev.* 43 (2) (Feb. 2008) 134–179, <https://doi.org/10.1080/05704920701829043>.
- [32] S. Kar, D.R. Katti, K.S. Katti, Fourier transform infrared spectroscopy based spectral biomarkers of metastasized breast cancer progression, *Spectrochim. Acta Part A Mol. Biomol. Spectrosc.* 208 (2019) 85–96, <https://doi.org/10.1016/j.saa.2018.09.052>.
- [33] D.L. Kitane, et al., A simple and fast spectroscopy-based technique for Covid-19 diagnosis, *Sci. Rep.* 11 (1) (2021) 1–11, <https://doi.org/10.1038/s41598-021-95568-5>.
- [34] B.R. da Cunha, L. Ramalhete, L.P. Fonseca, C.R.C. Calado, Fourier-Transform mid-infrared (FT-MIR) spectroscopy in biomedicine, in: Y. Tutar (Ed.), *Essential Techniques for Medical and Life Scientists: A Guide to Contemporary Methods and Current Applications- Part II*, Bentham Science Publisher, 2020, pp. 1–39, <https://doi.org/10.2174/9789911464867120010004>.
- [35] Y. Xiong, V. Shapaval, A. Kohler, J. Li, P.J. From, A fully automated robot for the preparation of fungal samples for FTIR spectroscopy using deep learning, *IEEE Access* 7 (2019) 132763–132774, <https://doi.org/10.1109/ACCESS.2019.2941704>.
- [36] M. Christensen, I. Chiciudean, P. Jablonski, A.-M. Tanase, V. Shapaval, H. Hansen, Towards high-throughput screening (HTS) of polyhydroxyalkanoate (PHA) production via Fourier transform infrared (FTIR) spectroscopy of Halomonas sp. R5-57 and Pseudomonas sp. MR4-99, *PLoS One* 18 (3) (Mar. 2023) e0282623, <https://doi.org/10.1371/journal.pone.0282623>.
- [37] M.J. Baker, et al., Using Fourier transform IR spectroscopy to analyze biological materials, *Nat. Protoc.* 9 (8) (Jul. 2014) 1771–1791, <https://doi.org/10.1038/nprot.2014.110>.
- [38] M.J. Baker, et al., Developing and understanding biofluid vibrational spectroscopy: a critical review, *Chem. Soc. Rev.* 45 (7) (2016) 1803–1818, <https://doi.org/10.1039/C5CS00585J>.
- [39] L. Sun, et al., Association between human blood metabolome and the risk of Alzheimer's disease, *Ann. Neurol.* 92 (5) (Nov. 2022) 756–767, <https://doi.org/10.1002/ana.26464>.
- [40] J.K. Frediani, et al., Metabolomics profiling in acute liver transplant rejection in a pediatric population, *Sci. Rep.* 12 (1) (Nov. 2022) 18663, <https://doi.org/10.1038/s41598-022-18957-4>.
- [41] S. Guan, et al., UPLC-Q-TOF/MS-Based plasma and urine metabolomics contribute to the diagnosis of sepsis, *J. Proteome Res.* 21 (1) (Jan. 2022) 209–219, <https://doi.org/10.1021/acs.jproteome.1c00777>.
- [42] J. Morze, et al., Metabolomics and type 2 diabetes risk: an updated systematic review and meta-analysis of prospective cohort studies, *Diabetes Care* 45 (4) (2022) 1013–1024, <https://doi.org/10.2337/dc21-1705>.
- [43] J. Kuligowski, et al., Infrared biospectroscopy for a fast qualitative evaluation of sample preparation in metabolomics, *Talanta* 127 (Sep. 2014) 181–190, <https://doi.org/10.1016/j.talanta.2014.04.009>.
- [44] T.A.H. Fonseca, et al., The impact of the serum extraction protocol on metabolomic profiling using UPLC-MS/MS and FTIR spectroscopy, *ACS Omega* 8 (23) (Jun. 2023) 20755–20766, <https://doi.org/10.1021/acsomega.3c01370>.
- [45] F.S. Cardoso, N. Germano, L. Bento, P. Fortuna, Time of admission to intensive care unit, strained capacity, and mortality: a retrospective cohort study, *J. Crit. Care* 54 (Dec. 2019) 1–6, <https://doi.org/10.1016/j.jcrc.2019.06.028>.
- [46] D. De Backer, et al., Challenges in the management of septic shock: a narrative review, *Intensive Care Med.* 45 (4) (Apr. 2019) 420–433, <https://doi.org/10.1007/s00134-019-05544-x>.
- [47] L.B. Brunker, C.S. Boncyk, K.F. Rengel, C.G. Hughes, Elderly patients and management in intensive care units (ICU): clinical challenges, *Clin. Interv. Aging* 18 (January) (Jan. 2023) 93–112, <https://doi.org/10.2147/CIA.S365968>.
- [48] D.M. Maslove, F. Lamontagne, J.C. Marshall, D.K. Heyland, A path to precision in the ICU, *Crit. Care* 21 (1) (Dec. 2017) 79, <https://doi.org/10.1186/s13054-017-1653-x>.
- [49] M.C. Chambers, et al., A cross-platform toolkit for mass spectrometry and proteomics, *Nat. Biotechnol.* 30 (10) (Oct. 2012) 918–920, <https://doi.org/10.1038/nbt.2377>.
- [50] H. Gowda, et al., Interactive XCMS online: simplifying advanced metabolomic data processing and subsequent statistical analyses, *Anal. Chem.* 86 (14) (Jul. 2014) 6931–6939, <https://doi.org/10.1021/ac500734c>.
- [51] Z.-J.J. Zhu, et al., Liquid chromatography quadrupole time-of-flight mass spectrometry characterization of metabolites guided by the METLIN database, *Nat. Protoc.* 8 (3) (Mar. 2013) 451–460, <https://doi.org/10.1038/nprot.2013.004>.
- [52] R. Tautenhahn, K. Cho, W. Uritboonthai, Z. Zhu, G.J. Patti, G. Siuzdak, An accelerated workflow for untargeted metabolomics using the METLIN database, *Nat. Biotechnol.* 30 (9) (Sep. 2012) 826–828, <https://doi.org/10.1038/nbt.2348>, 2012 309.
- [53] R. Tautenhahn, G.J. Patti, D. Rinehart, G. Siuzdak, XCMS online: a web-based platform to process untargeted metabolomic data, *Anal. Chem.* 84 (11) (Jun. 2012) 5035–5039, <https://doi.org/10.1021/ac300698c>.
- [54] Y. Lu, Z. Pang, J. Xia, Comprehensive investigation of pathway enrichment methods for functional interpretation of LC-MS global metabolomics data, *Briefings Bioinf.* 24 (1) (Jan. 2023), <https://doi.org/10.1093/BIB/BBAC553>.
- [55] Z. Pang, et al., Using MetaboAnalyst 5.0 for LC-HRMS spectra processing, multi-omics integration and covariate adjustment of global metabolomics data, *Nat. Protoc.* 17 (8) (Jun. 2022) 1735–1761, <https://doi.org/10.1038/s41596-022-00710-w>, 2022 178.
- [56] Z. Pang, et al., MetaboAnalyst 5.0: narrowing the gap between raw spectra and functional insights, *Nucleic Acids Res.* 49 (W1) (Jul. 2021) W388–W396, <https://doi.org/10.1093/NAR/GKAB382>.
- [57] Y. Yang, C. Cruickshank, M. Armstrong, S. Mahaffey, R. Reisdorff, N. Reisdorff, New sample preparation approach for mass spectrometry-based profiling of plasma results in improved coverage of metabolome, *J. Chromatogr. A* 1300 (2013) 217–226, <https://doi.org/10.1016/j.chroma.2013.04.030>.

- [58] I. Roberts, et al., Untargeted metabolomics of COVID-19 patient serum reveals potential prognostic markers of both severity and outcome, *Metabolomics* 18 (1) (Jan. 2022) 6, <https://doi.org/10.1007/s11306-021-01859-3>.
- [59] D. Sotello, S. Yang, K. Nugent, Glucose and lactate levels at admission as predictors of in-hospital mortality, *Cureus* 11 (10) (Oct. 2019), <https://doi.org/10.7759/cureus.6027>.
- [60] A.L. Mindikoglu, et al., Unique metabolic signature associated with hepatorenal dysfunction and mortality in cirrhosis, *Transl. Res.* 195 (May 2018) 25–47, <https://doi.org/10.1016/j.trsl.2017.12.002>.
- [61] M. Mierzchala-Pasierb, et al., Altered profiles of serum amino acids in patients with sepsis and septic shock – preliminary findings, *Arch. Biochem. Biophys.* 691 (Sep. 2020) 108508, <https://doi.org/10.1016/j.abb.2020.108508>.
- [62] H.-R. Chu, Z.A. Puthucheary, Amino acid turnover, protein metabolism, and nitrogen balance in acute kidney injury, in: *Critical Care Nephrology*, third ed., Elsevier, 2019, pp. 434–442.e2, <https://doi.org/10.1016/B978-0-323-44942-7.00074-1>.
- [63] O. Rooyackers, R. Koucké-Zadeh, I. Tjäder, Å. Norberg, M. Klaude, J. Werner, Whole body protein turnover in critically ill patients with multiple organ failure, *Clin. Nutr.* 34 (1) (Feb. 2015) 95–100, <https://doi.org/10.1016/j.clnu.2014.01.020>.
- [64] G. Kaur, X. Ji, I. Rahman, SARS-CoV2 infection alters tryptophan catabolism and phospholipid metabolism, *Metabolites* 11 (10) (Sep. 2021) 659, <https://doi.org/10.3390/metabo11100659>.
- [65] I. Klobucar, et al., Low valine serum levels predict increased 1-year mortality in acute heart failure patients, *Biomolecules* 13 (9) (Aug. 2023) 1323, <https://doi.org/10.3390/biom13091323>.
- [66] M.A. Puskarich, C. McHugh, T.L. Flott, A. Karnovsky, A.E. Jones, K.A. Stringer, Serum levels of branched chain amino acids predict duration of cardiovascular organ failure in septic shock, *Shock* 56 (1) (Jul. 2021) 65–72, <https://doi.org/10.1097/SHK.0000000000001687>.
- [67] Y. Ding, Y. Zhang, W. Zhang, J. Shang, Z. Xie, C. Chen, Effects of lipoic acid on ischemia-reperfusion injury, *Oxid. Med. Cell. Longev.* 2021 (Oct. 2021) 1–15, <https://doi.org/10.1155/2021/5093216>.
- [68] L. Rochette, S. Ghibu, Mechanics insights of alpha-lipoic acid against cardiovascular diseases during COVID-19 infection, *Int. J. Mol. Sci.* 22 (15) (Jul. 2021) 7979, <https://doi.org/10.3390/ijms22157979>.
- [69] M. Bruegel, et al., Sepsis-associated changes of the arachidonic acid metabolism and their diagnostic potential in septic patients, *Crit. Care Med.* 40 (5) (May 2012) 1478–1486, <https://doi.org/10.1097/CCM.0b013e3182416f05>.
- [70] J. Yamaguchi, K. Kinoshita, S. Ihara, M. Furukawa, A. Sakurai, The clinical significance of low serum arachidonic acid in sepsis patients with hypoalbuminemia, *Intern. Med.* 57 (13) (Jul. 2018) 1833–1840, <https://doi.org/10.2169/internalmedicine.9124-17>.
- [71] S. Ouchi, et al., Low docosahexaenoic acid, dihomo-gamma-linolenic acid, and arachidonic acid levels associated with long-term mortality in patients with acute decompensated heart failure in different nutritional statuses, *Nutrients* 9 (9) (Aug. 2017) 956, <https://doi.org/10.3390/nu9090956>.
- [72] Q. Wang, et al., O-GlcNAc transferase promotes influenza A virus-induced cytokine storm by targeting interferon regulatory factor-5, *Sci. Adv.* 6 (16) (Apr. 2020) 1–14, <https://doi.org/10.1126/sciadv.aaz7086>.
- [73] A. Thoof, R. Conotte, J.-M. Colet, K. Zouaoui Boudjeltia, P. Biston, M. Piagnerelli, Serum metabolomic profiles in critically ill patients with shock on admission to the intensive care unit, *Metabolites* 13 (4) (Apr. 2023) 523, <https://doi.org/10.3390/metabo13040523>.
- [74] A.J. Rogers, et al., Metabolomic derangements are associated with mortality in critically ill adult patients, *PLoS One* 9 (1) (Jan. 2014) e87538, <https://doi.org/10.1371/journal.pone.0087538>.
- [75] Y. Wang, et al., Urinary metabolic study of patients with acute coronary syndrome using UPLC-QTOF/MS, *J. Chromatogr. B* 1100–1101 (August) (Nov. 2018) 122–130, <https://doi.org/10.1016/j.jchromb.2018.10.005>.
- [76] W. Jin, et al., Hepatoprotective effects of ixeris chinensis on nonalcoholic fatty liver disease induced by high-fat Diet in mice: an integrated gut microbiota and metabolic analysis, *Molecules* 27 (10) (May 2022) 3148, <https://doi.org/10.3390/molecules27103148>.
- [77] N. Pouporé, R. Chosed, S. Arce, R. Rainer, R.L. Goodwin, T.I. Nathaniel, Metabolomic profiles of men and women ischemic stroke patients, *Diagnostics* 11 (10) (Sep. 2021) 1786, <https://doi.org/10.3390/diagnostics11101786>.
- [78] W.R. Wikoff, et al., Metabolomic markers of altered nucleotide metabolism in early stage adenocarcinoma, *Cancer Prev. Res.* 8 (5) (May 2015) 410–418, <https://doi.org/10.1158/1940-6207.CAPR-14-0329>.
- [79] C. Chen, X. Meng, Y. Zhu, J. Zhang, R. Wang, Early identification of serum biomarkers and pathways of sepsis through GC-MS-based metabolomics analysis, *Front. Biosci.* 28 (7) (Jul. 2023) 145, <https://doi.org/10.31083/j.fbl2807145>.
- [80] A.G. Vassiliou, et al., Serum coenzyme Q10 levels are decreased in critically-ill septic patients: results from a preliminary study, *Biol. Res. Nurs.* 23 (2) (Apr. 2021) 198–207, <https://doi.org/10.1177/1099800420944489>.
- [81] N.V. Beloborodova, A.Y. Olenin, A.K. Pautova, Metabolomic findings in sepsis as a damage of host-microbial metabolism integration, *J. Crit. Care* 43 (Feb. 2018) 246–255, <https://doi.org/10.1016/j.jcrc.2017.09.014>.
- [82] C. Li, et al., Prognostic value of elevated levels of plasma N-acetylneurameric acid in patients with heart failure, *Circ. Hear. Fail.* 14 (11) (Nov. 2021) E008459, <https://doi.org/10.1161/CIRCHEARTFAILURE.121.008459>.
- [83] C. Zhang, J. Chen, Y. Liu, D. Xu, Sialic acid metabolism as a potential therapeutic target of atherosclerosis, *Lipids Health Dis.* 18 (1) (Dec. 2019) 173, <https://doi.org/10.1186/s12944-019-1113-5>.
- [84] T. Kimura, et al., Identification of biomarkers for development of end-stage kidney disease in chronic kidney disease by metabolomic profiling, *Sci. Rep.* 6 (1) (May 2016) 26138, <https://doi.org/10.1038/srep26138>.
- [85] Y. Sun, R. Chatterjee, A. Ronanki, K. Ye, Circulating polyunsaturated fatty acids and COVID-19: a prospective cohort study and mendelian randomization analysis, *Front. Med.* 9 (June) (Jun. 2022) 1–12, <https://doi.org/10.3389/fmed.2022.923746>.
- [86] A. Mazidimoradi, E. Alemzadeh, H. Salehiniya, The effect of polyunsaturated fatty acids on the severity and mortality of COVID patients, *syste. review* (Jun. 2022), <https://doi.org/10.1016/j.jifs.2022.120489>.
- [87] R.J. Cardwell, R.H. Birkhahn, K.A. Crist, E.M. Lee, N.R. Thomford, Palmitate and stearate kinetics in the rat during sepsis and trauma, *J. Surg. Res.* 50 (1) (Jan. 1991) 51–56, [https://doi.org/10.1016/0022-4804\(91\)90009-B](https://doi.org/10.1016/0022-4804(91)90009-B).
- [88] M.J. Hubler, A.J. Kennedy, Role of lipids in the metabolism and activation of immune cells, *J. Nutr. Biochem.* 34 (1) (Aug. 2016) 1–7, <https://doi.org/10.1016/j.jnutbio.2015.11.002>.
- [89] H. Miao, et al., Stearic acid induces proinflammatory cytokine production partly through activation of lactate-HIF1 α pathway in chondrocytes, *Sci. Rep.* 5 (1) (Aug. 2015) 13092, <https://doi.org/10.1038/srep13092>.
- [90] S.A. van den Berg, et al., High levels of dietary stearate promote adiposity and deteriorate hepatic insulin sensitivity, *Nutr. Metab.* 7 (1) (Dec. 2010) 24, <https://doi.org/10.1186/1743-7075-7-24>.
- [91] S. Montazeraheb, et al., COVID-19 infection: an overview on cytokine storm and related interventions, *Virol.* 19 (1) (May 2022) 92, <https://doi.org/10.1186/s12985-022-01814-1>.
- [92] R.H. Meacham, E.R. Bowman, H. McKennis, Additional routes in the metabolism of nicotine to 3-pyridylacetate, *J. Biol. Chem.* 247 (3) (Feb. 1972) 902–908, [https://doi.org/10.1016/S0021-9258\(19\)45692-5](https://doi.org/10.1016/S0021-9258(19)45692-5).
- [93] K. Pei, J. Ou, J. Huang, S. Ou, p-Coumaric acid and its conjugates: dietary sources, pharmacokinetic properties and biological activities, *J. Sci. Food Agric.* 96 (9) (Jul. 2016) 2952–2962, <https://doi.org/10.1002/jsfa.7578>.
- [94] X. Yang, et al., Simultaneous determination of multiple components in rat plasma by UHPLC-sMRM for pharmacokinetic studies after oral administration of Qingjin Yiqi Granules, *Front. Pharmacol.* 14 (April) (Apr. 2023), <https://doi.org/10.3389/fphar.2023.1155973>.
- [95] T.N. Souza, et al., Local administration of p-coumaric acid decreases lipopolysaccharide-induced acute lung injury in mice: in vitro and in silico studies, *Eur. J. Pharmacol.* 897 (November 2020) (Apr. 2021) 173929, <https://doi.org/10.1016/j.ejphar.2021.173929>.
- [96] K. Kochan, et al., Infrared spectroscopy of blood, *Appl. Spectrosc.* 75 (6) (Jun. 2021) 611–646, <https://doi.org/10.1177/0003702820985856>.
- [97] A. Rohman, A. Windarsih, E. Lukitaningsih, M. Rafi, K. Betania, N.A. Fadzillah, The use of FTIR and Raman spectroscopy in combination with chemometrics for analysis of biomolecules in biomedical fluids: a review, *Biomed. Spectrosc. Imag.* 8 (3–4) (Jan. 2020) 55–71, <https://doi.org/10.3233/BSI-200189>.
- [98] X. Wang, et al., A study of Parkinson's disease patients' serum using FTIR spectroscopy, *Infrared Phys. Technol.* 106 (December 2019) (May 2020) 103279, <https://doi.org/10.1016/j.infrared.2020.103279>.
- [99] V. Rai, et al., Serum-based diagnostic prediction of oral submucous fibrosis using FTIR spectrometry, *Spectrochim. Acta Part A Mol. Biomol. Spectrosc.* 189 (Jan. 2018) 322–329, <https://doi.org/10.1016/j.saa.2017.08.018>.
- [100] N. Mateus Pereira de Souza, et al., Detection of metabolic syndrome with ATR-FTIR spectroscopy and chemometrics in blood plasma, *Spectrochim. Acta Part A Mol. Biomol. Spectrosc.* 288 (September 2022) (Mar. 2023) 122135, <https://doi.org/10.1016/j.saa.2022.122135>.
- [101] C. Lacombe, V. Untereiner, C. Gobinet, M. Zater, G.D. Sockalingum, R. Garnotel, Rapid screening of classic galactosemia patients: a proof-of-concept study using high-throughput FTIR analysis of plasma, *Analyst* 140 (7) (2015) 2280–2286, <https://doi.org/10.1039/C4AN01942C>.
- [102] A. Nunes, FTIR spectroscopy - a potential tool to identify metabolic changes in dementia patients, *Alzheimer's Neurodegener. Dis.* 2 (2) (Dec. 2016) 1–9, <https://doi.org/10.24966/AND-9608/100007>.
- [103] A.-Z. Ma, S. Amh, M. Ra, A.K. Ma, Diagnosis of patients with hypothyroidism using spectrochemical analysis of blood sera, *La Prensa Med. Argenti.* 105 (6) (2019) 1–8, <https://doi.org/10.47275/0032-745X-250>.
- [104] S. Taleb, et al., Predictive biomarkers of intensive care unit and mechanical ventilation duration in critically-ill Coronavirus disease 2019 patients, *Front. Med.* 8 (Aug. 2021) 733657, <https://doi.org/10.3389/fmed.2021.733657>.
- [105] O.J. McElvaney, et al., Characterization of the inflammatory response to severe COVID-19 illness, *Am. J. Respir. Crit. Care Med.* 202 (6) (Sep. 2020) 812–821, <https://doi.org/10.1164/rccm.202005-1583OC>.
- [106] C.E. Cox, Persistent systemic inflammation in chronic critical illness, *Respir. Care* 57 (6) (Jun. 2012) 859–866, <https://doi.org/10.4187/respca.01719>.
- [107] C. Pommié, S. Levadoux, R. Sabatier, G. Lefranc, M.-P. Lefranc, IMGT standardized criteria for statistical analysis of immunoglobulin V-REGION amino acid properties, *J. Mol. Recogn.* 17 (1) (Jan. 2004) 17–32, <https://doi.org/10.1002/jmr.647>.
- [108] Y. Wang, M. Hu, H. Yang, Cirrhosis is an independent predictor for COVID-19 mortality: a meta-analysis of confounding cofactors-controlled data, *J. Hepatol.* 78 (1) (Jan. 2023) e28–e31, <https://doi.org/10.1016/j.jhep.2022.09.015>.
- [109] I. Vujić, Outcomes of COVID-19 among patients with liver disease, *World J. Gastroenterol.* 29 (5) (Feb. 2023) 815–824, <https://doi.org/10.3748/WJG.V29.I5.815>.
- [110] M. Akpe, Does COVID-19 cause hypertension? *Angiology* 73 (7) (Aug. 2022) 682, <https://doi.org/10.1177/00033197211053903>.